

Effective longitudinal shear moduli of periodic fibre-reinforced composites with radially-graded fibres

Edoardo Artioli, Paolo Bisegna*, Franco Maceri

Department of Civil Engineering, University of Rome "Tor Vergata", via del Politecnico 1, 00133 Rome, Italy

ARTICLE INFO

Article history:

Received 22 May 2009

Received in revised form 11 September 2009

Available online 13 October 2009

Keywords:

Micromechanics

Fibre-reinforced composite materials

Functionally graded materials

Asymptotic homogenization

Analytical solutions

Complex variable

Stress concentrations

ABSTRACT

This paper presents a closed-form expression for the homogenized longitudinal shear moduli of a linear elastic composite material reinforced by long, parallel, radially-graded circular fibres with a periodic arrangement. An imperfect linear elastic fibre-matrix interface is allowed. The asymptotic homogenization method is adopted, and the relevant cell problem is addressed. Periodicity is enforced by resorting to the theory of Weierstrass elliptic functions. The equilibrium equation in the fibre domain is solved in closed form by applying the theory of hypergeometric functions, for new wide classes of grading profiles defined in terms of special functions. The effectiveness of the present analytical procedure is proved by convergence analysis and comparison with finite element solutions. A parametric analysis investigating the influence of microstructural and material features on the effective moduli is presented. The feasibility of mitigating the shear stress concentration in the composite by tuning the fibre grading profile is shown.

© 2009 Elsevier Ltd. All rights reserved.

1. Introduction

Graded materials are substances having composition, micro-structure and properties which vary continuously in space (Suresh, 1997, 2001). Their outstanding merit is that their properties can be tailored via the design of the gradients.

Graded composites consist of inclusions, either of spatially variable volume fractions (Reiter et al., 1997; Genin and Birman, 2009), or made of graded materials (Gu and Yu, 2003), embedded in a homogeneous host matrix. This work, dealing with the latter kind of graded composites, is aimed at determining the effective longitudinal shear moduli of linear elastic, periodic composites, reinforced by radially-graded long fibres. Its significance, for the development of engineering components, relies on the fact that properly tuning the fibre grading profile allows to modulate the material stress state, thus enhancing material performance and durability.

The analysis is developed within the framework of antiplane shear deformations, and the asymptotic homogenization method is adopted (Bensoussan et al., 1978; Sanchez-Palencia, 1980; Kalamkarov, 1992). It hinges on the so-called cell (or local) problem, whose major issues are: (i) the solution of the equilibrium field equation in the radially-graded fibre domain; (ii) the satisfaction

of the equilibrium and interface-constitution laws at the fibre-matrix interface; and (iii) the satisfaction of the periodic boundary conditions at the unit-cell boundary.

The first issue is the central one in the theory of graded materials. Most of the interest in the literature has focused on graded plates, but several closed-form solutions are available for radially-graded cylinders or spheres, mainly with reference to electric or thermal conduction problems, or electrostatics. Those results carry over to the present case, since antiplane shear deformation is governed by formally identical equations. In particular, limiting the literature review to graded cylinders, power-law (r^k), linear ($b + r$), and exponential (e^{br}) profiles were considered by Gu and Yu (2003), Wei et al. (2003) and Chen and Kuo (2005), where r is the radial coordinate along the fibre radius; the more general profile $(b + r)^k e^{br}$ was considered by Wei et al. (2006). In this work, besides the grading profile e^{br} , previously studied by Martin (2002) for spheres and considered here with reference to cylinders, closed-form solutions for wide families of grading profiles are derived in a systematic manner, exploiting an idea presented in Section 4.3. In particular, solutions for grading profiles given by the square of Bessel functions, or involving the square of hypergeometric functions, are obtained. Many of the previously cited grading profiles are recovered as particular cases, and new variants are allowed, including, e.g., the square of Chebyshev or Legendre's polynomials, or involving logarithmic or trigonometric functions. To the best of the authors' knowledge, a closed-form solution for such grading formats appears here for the first time. Such a collection of

* Corresponding author. Tel.: +39 06 7259 7079; fax: +39 06 7259 7005.

E-mail addresses: artioli@ing.uniroma2.it (E. Artioli), bisegna@uniroma2.it (P. Bisegna), franco.maceri@lagrange.it (F. Maceri).

analytical profiles can be useful as a benchmark for numerical solutions, and, mainly, both to approximate experimental profiles encountered in applications and to devise new graded composites with enhanced performances in the field of antiplane shear deformations, electric or thermal conduction, or electrostatics.

Interfaces between fibres and matrix are usually assumed to be perfect, i.e., continuity of both the displacement and traction vectors is enforced. In this work, imperfect interfaces are considered and modeled with the simple and popular zero-thickness, linear spring-layer model. In particular, a displacement discontinuity linearly related to the interface traction in terms of a spring constant parameter is allowed at interfaces (Lene and Leguillon, 1982; Hashin, 1991; Bigoni et al., 1998). The case of perfect interfaces is recovered by letting the interface parameter go to infinity. The present analysis could be extended to more general interface models (Benveniste and Miloh, 2001; Hashin, 2002), or to the case of inclusions coated with homogeneous interface (Nicorovici et al., 1993; Gu and Yu, 2003) or graded interface (Kanaun and Kudriavtseva, 1989; Herve and Zaoui, 1993; Lutz and Zimmerman, 1996, 2005; Shen and Li, 2003, 2005; Sevostianov and Kachanov, 2007).

Many procedures for estimating the effective moduli of composites are available in the literature. Some of them are based on the solution for dilute suspensions, whereas others take approximately into account interactions among fibres (see, e.g., Mura (1987) and Milton (2004) and the references cited therein). For periodic microstructures, these interactions are rigorously taken into account by imposing periodic boundary conditions at the unit-cell boundary. This issue can be accomplished by using different methods, including Fourier transform (Iwakuma and Nemat-Nasser, 1983; Michel et al., 1999; Bonnet, 2007), elastostatic resonances (Kantor and Bergman, 1982), boundary elements (Helsing, 1995), finite elements (Michel et al., 1999; Shabana and Noda, 2008). In this work, periodicity is enforced following an approach tracing back to the classical multipole expansion method (Rayleigh, 1892), quite popular in the literature (Perrins et al., 1979; Kalamkarov, 1992; Meguid and Kalamkarov, 1994; Rodríguez-Ramos et al., 2001; Jiang et al., 2004; Chen and Kuo, 2005; Parnell and Abrahams, 2006; Bisegna and Caselli, 2008; Kushch et al., 2008). In particular, the cell function over the matrix domain is represented as a series of doubly-periodic functions built up by resorting to the theory of Weierstrass elliptic functions (Whittaker and Watson, 1927; Apostol, 1997), naturally satisfying the periodicity condition at the cell boundary. The actual solution is then computed through the identification of the latter representation, with the Fourier-series representation arising after satisfying the equilibrium field equations in the fibre and matrix domains, and enforcing the equilibrium and interface-constitution laws at the fibre-matrix interface. An infinite system of linear algebraic equations is thus obtained, which is truncated to a finite order N and solved. Closed-form formulas are obtained to the truncation orders $N = 1$ and $N = 2$ for general unit cell microgeometries with oblique unequal sides, and to any truncation order N for rectangular microgeometries.

The outline of the paper is as follows. In Section 2 the mathematical statement of the problem under consideration is introduced and the homogenized equation is presented; Section 3 focuses on the cell problem and the relative solution strategy. In Section 4 closed-form solutions are obtained for different types of fibre grading profiles. Section 5 reports a campaign of numerical tests aimed at both validating the present results and at showing the influence of the grading features and unit cell geometry on the overall elastic behaviour of the composite. Moreover, a comparison with other homogenization approaches available in the literature (Kanaun and Kudriavtseva, 1989; Sevostianov and Kachanov, 2007) is presented. Finally, the feasibility of mitigating

the shear stress concentration in the composite by tuning the fibre grading profile is investigated.

2. Statement of the problem

Reference is made to a composite material constituted of long, parallel fibres with circular cross-section, embedded into a surrounding matrix. Fibres are arranged in a regular lattice determined by two families of parallel lines, respectively, parallel to the x_1 -axis, and forming an angle φ with the latter, as sketched in Fig. 1(a). This geometrical set up can be interpreted as a two dimensional array of unit cells, developing periodically along the x_1 and φ directions. The unit cell, i.e., the micro-structure of the composite, can be appreciated in Fig. 1(b). The cell sides measure L_1 and L_2 , respectively, and the fibre radius is R .

The effective material shear moduli are obtained here by asymptotic homogenization: to this end, a family of problems is introduced, indexed by a parameter ε scaling the microstructure (Fig. 1(a)). The homogenization limit is obtained by letting ε go to zero.

In the framework of antiplane shear deformations, the problem of determining the longitudinal displacement field w_ε in the composite domain is stated as follows:

$$\operatorname{div}(\mathbf{G}\nabla w_\varepsilon) = 0, \quad \text{in } \Omega_\varepsilon^f \cup \Omega_\varepsilon^m; \quad (1)$$

$$[[\mathbf{G}\nabla w_\varepsilon \cdot \mathbf{v}]] = 0, \quad \text{on } \Gamma_\varepsilon; \quad (2)$$

$$\mathbf{G}\nabla w_\varepsilon \cdot \mathbf{v} = \frac{1}{\varepsilon} D[[w_\varepsilon]], \quad \text{on } \Gamma_\varepsilon. \quad (3)$$

Here Ω_ε^f and Ω_ε^m denote fibre and matrix domains, respectively, Γ_ε is the ensemble of fibre-matrix interfaces, \mathbf{v} is the normal unit vector to Γ_ε pointing into Ω_ε^m , and square brackets $[[\cdot]]$ denote the jump of the enclosed quantity across the interface, defined as extra-fibre value minus intra-fibre value.

Eq. (1) is the field equilibrium equation; Eq. (2) accounts for equilibrium at the fibre-matrix interface, stipulating the continuity of the normal-to-interface component of the shear stress; and Eq. (3) describes the interface constitution law. These equations must be complemented by suitable boundary conditions on the boundary of the domain $\Omega = \Omega_\varepsilon^f \cup \Gamma_\varepsilon \cup \Omega_\varepsilon^m$, but their specification is immaterial for the present treatment.

Fibres and matrix are assumed to be linear elastic, and their shear moduli are collected in the constitutive tensor \mathbf{G} , which specializes in

$$\mathbf{G} = \mathbf{G}^f, \quad \text{in } \Omega_\varepsilon^f, \quad \mathbf{G} = \mathbf{G}^m, \quad \text{in } \Omega_\varepsilon^m. \quad (4)$$

The matrix material is homogeneous and isotropic, so that $\mathbf{G}^m = G^m \mathbf{I}$, with \mathbf{I} the second order identity tensor and G^m the matrix shear modulus. Fibres are made of a linear elastic, cylindrically-orthotropic material whose moduli are functionally-graded along

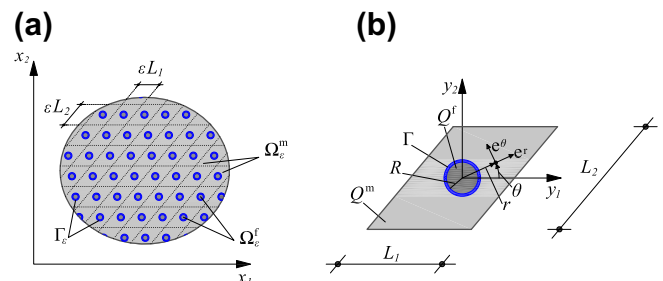


Fig. 1. (a) Geometrical setting of the problem at the macroscale: cross-section of the fibrous composite (the fibre size is exaggerated with respect to the sample size, for illustrative purposes; the fibre-matrix interface has zero thickness). (b) Geometrical setting of the cell (or local) problem at the microscale.

the radius. Introducing a polar coordinate system (O, r, θ) as depicted in Fig. 1(b), the fibre elasticity tensor is:

$$\mathbf{G}^f = (G^r \mathbf{e}^r \otimes \mathbf{e}^r + G^\theta \mathbf{e}^\theta \otimes \mathbf{e}^\theta) g(\rho), \quad (5)$$

where

$$\rho = \frac{r}{R} \quad (6)$$

is the radial dimensionless coordinate, \mathbf{e}^r and \mathbf{e}^θ are the radial and tangential unit vectors, respectively, \otimes denotes the tensor product, and the dimensionless function $g(\rho)$ expresses the material grading law along the radial direction. Accordingly, $G^r g(0)$ and $G^\theta g(0)$ [respectively, $G^r g(1)$ and $G^\theta g(1)$] are the radial and tangential shear moduli at the fibre axis [respectively, boundary].

Fibre-matrix interfaces are assumed to have zero-thickness and to be imperfect. The linear spring-layer model, linearly relating the displacement discontinuity $[[w_\varepsilon]]$ to the interface traction $\mathbf{G} \nabla w_\varepsilon \cdot \mathbf{v}$, in terms of the spring constant parameter D is adopted (Lene and Leguillon, 1982; Hashin, 1991; Bigoni et al., 1998). As a matter of fact, interfaces have a physical thickness t which, though much smaller than the microstructural length scales L_1 and L_2 to justify the present zero-thickness model, rescales as the latter ones during the homogenization process (Fig. 1(a)). Recalling that the corresponding interface parameter is inversely proportional to the interface thickness, the ε^{-1} scaling of the interface parameter in the homogenization limit follows (Lene and Leguillon, 1982; Amar et al., 2006).

In order to guarantee the well posedness of the above problem, the following hypotheses are assumed:

$$G^m > 0, \quad G^r > 0, \quad G^\theta > 0, \quad D > 0, \quad g(\rho) > 0, \quad \text{in } (0, 1]. \quad (7)$$

2.1. Homogenized equilibrium equation

The asymptotic homogenization method is employed to derive the homogenized or effective constitutive tensor of the composite material. It is only sketched here for the sake of completeness. The interested Reader may refer, e.g., to Bensoussan et al. (1978) and Sanchez-Palencia (1980).

As shown in Fig. 1(a), two different length scales characterize the problem under consideration. Hence, two different space variables are introduced: the macroscopic one, x , and the microscopic one, $y = x/\varepsilon$, $y \in Q$, being Q the unit cell (see Fig. 1(b)), whose intra-fibre space, extra-fibre space and fibre-matrix interface are denoted by Q^f , Q^m and Γ , respectively. Accordingly, the divergence and gradient operators are given by the following relations:

$$\text{div} = \text{div}_x + \frac{1}{\varepsilon} \text{div}_y, \quad \nabla = \nabla_x + \frac{1}{\varepsilon} \nabla_y. \quad (8)$$

An asymptotic expansion of the unknown displacement field is considered in the form:

$$w_\varepsilon(x, y) = w_0(x, y) + \varepsilon w_1(x, y) + \varepsilon^2 w_2(x, y) + \dots, \quad (9)$$

where w_0 , w_1 , w_2 are Q -periodic functions in y , and w_1 , w_2 have null integral average over Q . Substituting (9) into Problem (1)–(3) and equating the power-like terms of ε , three differential problems for w_0 , w_1 and w_2 are obtained, respectively. The problem for w_0 is:

$$\text{div}_y(\mathbf{G} \nabla_y w_0) = 0, \quad \text{in } Q^f \cup Q^m; \quad (10)$$

$$[[\mathbf{G} \nabla_y w_0 \cdot \mathbf{v}]] = 0, \quad \text{on } \Gamma; \quad (11)$$

$$\mathbf{G} \nabla_y w_0 \cdot \mathbf{v} = D[[w_0]], \quad \text{on } \Gamma. \quad (12)$$

Problem (10)–(12), taking into account (7), implies that $w_0 = w_0(x)$ (Lene and Leguillon, 1982). The problem for w_1 is:

$$\text{div}_y[\mathbf{G}(\nabla_y w_1 + \nabla_x w_0)] = 0, \quad \text{in } Q^f \cup Q^m; \quad (13)$$

$$[[\mathbf{G}(\nabla_y w_1 + \nabla_x w_0) \cdot \mathbf{v}]] = 0, \quad \text{on } \Gamma; \quad (14)$$

$$\mathbf{G}(\nabla_y w_1 + \nabla_x w_0) \cdot \mathbf{v} = D[[w_1]], \quad \text{on } \Gamma. \quad (15)$$

The unknown function w_1 is represented in the form (Bensoussan et al., 1978; Sanchez-Palencia, 1980):

$$w_1(x, y) = -\chi(y) \cdot \nabla_x w_0(x), \quad (16)$$

where the cell function $\chi(y)$ has been introduced. Its components χ_h , $h = 1, 2$, are the unique, null average, Q -periodic solutions of the cell problem:

$$\text{div}_y[\mathbf{G}(\nabla_y \chi_h - \mathbf{e}_h)] = 0, \quad \text{in } Q^f \cup Q^m; \quad (17)$$

$$[[\mathbf{G}(\nabla_y \chi_h - \mathbf{e}_h) \cdot \mathbf{v}]] = 0, \quad \text{on } \Gamma; \quad (18)$$

$$\mathbf{G}(\nabla_y \chi_h - \mathbf{e}_h) \cdot \mathbf{v} = D[[\chi_h]], \quad \text{on } \Gamma, \quad (19)$$

where \mathbf{e}_h is the unit vector parallel to the y_h -axis.

Finally, the problem for w_2 is obtained:

$$\text{div}_y[\mathbf{G}(\nabla_y w_2 + \nabla_x w_1)] = -\text{div}_x[\mathbf{G}(\nabla_y w_1 + \nabla_x w_0)], \quad \text{in } Q^f \cup Q^m; \quad (20)$$

$$[[\mathbf{G}(\nabla_y w_2 + \nabla_x w_1) \cdot \mathbf{v}]] = 0, \quad \text{on } \Gamma; \quad (21)$$

$$\mathbf{G}(\nabla_y w_2 + \nabla_x w_1) \cdot \mathbf{v} = D[[w_2]], \quad \text{on } \Gamma. \quad (22)$$

Integrating (20) both in Q^f and in Q^m , using the Gauss–Green Lemma, adding the two contributions and exploiting (21), the following equation is obtained:

$$\frac{1}{|Q|} \int_{Q^f \cup Q^m} \text{div}_x[\mathbf{G}(\nabla_y w_1 + \nabla_x w_0)] da = 0, \quad (23)$$

where da is the area element of $Q^f \cup Q^m$ and $|\cdot|$ is the Lebesgue measure. Substituting (16) into (23), the homogenized equation for the macroscopic displacement w_0 is finally derived:

$$\text{div}_x(\mathbf{G}^\# \nabla_x w_0) = 0. \quad (24)$$

Here $\nabla_x w_0$ is the macroscopic shear strain, and

$$\mathbf{G}^\# = \frac{1}{|Q|} \int_{Q^f \cup Q^m} \mathbf{G}(\mathbf{I} - \nabla_y^t \chi) da \quad (25)$$

is the effective constitutive tensor, where the superscript ‘t’ denotes the transpose. Using the Gauss–Green Lemma, (25) is transformed into:

$$\begin{aligned} \mathbf{G}^\# &= (1-f)\mathbf{G}^m + \frac{1}{|Q|} \int_{Q^f} \mathbf{G}^f da + \frac{1}{|Q|} \int_{Q^f} (\text{div}_y \mathbf{G}^f) \otimes \chi da \\ &\quad + \frac{1}{|Q|} \int_{\Gamma} [[\mathbf{G} \mathbf{v} \otimes \chi]] dl, \end{aligned} \quad (26)$$

where $f = \pi R^2/|Q|$ is the fibre volume fraction, and dl is the line element of Γ . The preceding equation for $\mathbf{G}^\#$ can be rewritten in terms of the auxiliary cell function:

$$\tilde{\chi} = \chi - (y_1 \mathbf{e}_1 + y_2 \mathbf{e}_2) \quad (27)$$

as follows:

$$\mathbf{G}^\# = \mathbf{G}^m + \frac{1}{|Q|} \int_{Q^f} (\text{div}_y \mathbf{G}^f) \otimes \tilde{\chi} da + \frac{1}{|Q|} \int_{\Gamma} [[\mathbf{G} \mathbf{v} \otimes \tilde{\chi}]] dl. \quad (28)$$

Eq. (28) yields the effective shear moduli of the composite material in terms of the solution χ of the cell problem. The cell function is involved with the particular form assumed for \mathbf{G}^f and, in the following sections, is derived in closed form for a set of different choices of the fibre constitutive law.

In applications, a central role is played by the local shear stress $\tau_\varepsilon = \mathbf{G} \nabla w_\varepsilon$ in the composite. The leading-order term of its asymptotic expansion turns out to be:

$$\tau_0 = \mathbf{G}(\nabla_x w_0 + \nabla_y w_1) = \mathbf{G}(\mathbf{I} - \nabla_y^t \chi) [\nabla_x w_0]. \quad (29)$$

This expression will be used in Section 5.4, dealing with stress concentration issues.

3. Cell problem

3.1. Fourier series representation

The general solution of the field equation (17) is obtained via the following Fourier series representation:

- in the isotropic, homogeneous matrix subdomain Q^m

$$\chi_h(r, \theta)|_{Q^m} := \chi_h^m(r, \theta) = y_h + \Re \left[\sum_{k=-\infty}^{+\infty} b_{kh} \rho^k e^{ik\theta} \right], \quad (30)$$

- in the cylindrically orthotropic, radially-graded fibre subdomain Q^f

$$\chi_h(r, \theta)|_{Q^f} := \chi_h^f(r, \theta) = y_h + \Re \left[\sum_{k=1}^{+\infty} a_{kh} W_k(\rho) e^{ik\theta} \right]. \quad (31)$$

Here $i = \sqrt{-1}$; the symbol \Re denotes the real part; the sums affected by the apex $^\circ$, are extended over odd indices only, since the microstructure considered herein (Fig. 1) is centre symmetric with respect to the origin O , so that the solution χ satisfies the property:

$$\chi(r, \theta) = -\chi(r, \theta + \pi). \quad (32)$$

Moreover, the sum in (31) is extended over positive indices only, in order to enforce the regularity of χ_h near $O \in Q^f$. The functions $W_k(\rho)$ solve the problem:

$$W_k'' + \left(\frac{g'}{g} + \frac{1}{\rho} \right) W_k' - \frac{\sigma^2 k^2}{\rho^2} W_k = 0, \quad \text{in } (0, 1), \quad (33)$$

$$W_k(0) = 0, \quad (34)$$

$$W_k(1) = 1, \quad (35)$$

where (34) is a regularity requirement on W_k , (35) is a normalization condition, $\sigma^2 = G^0/G^r$ is the anisotropy ratio, and an apex denotes differentiation with respect to ρ . Finally, the quantities a_{kh} , b_{kh} , $b_{(-k)h}$, $k = 1, \dots, +\infty$, odd k , are complex constants which are determined in Sections 3.2 and 3.3, by exploiting the interface boundary conditions (18) and (19) on Γ and the periodicity requirement on ∂Q .

3.2. Interface boundary condition

Substituting the representations (30) and (31) into the interface boundary conditions (18) and (19), the following equations are obtained, for odd k , and $h = 1, 2$:

$$G^m k R^{-1} (b_{kh} - \bar{b}_{(-k)h}) = G^r g(1) W_k'(1) R^{-1} a_{kh}, \quad (36)$$

$$D(b_{kh} + \bar{b}_{(-k)h} - a_{kh}) = G^r g(1) W_k'(1) R^{-1} a_{kh}, \quad (37)$$

where an overbar denotes the complex conjugate. Eqs. (36) and (37) allow to express the unknown coefficients a_{kh} and b_{kh} as functions of $b_{(-k)h}$, as follows:

$$a_{kh} = \lambda_k \bar{b}_{(-k)h}, \quad b_{kh} = \gamma_k \bar{b}_{(-k)h}, \quad (38)$$

where

$$\lambda_k = \frac{2RD[G^r g(1)]^{-1}}{k + \psi_k^-} \frac{k}{W_k'(1)}, \quad \gamma_k = \frac{k + \psi_k^+}{k + \psi_k^-}, \quad (39)$$

being

$$\psi_k^\pm = RD \left\{ \frac{k}{W_k'(1)} [G^r g(1)]^{-1} \pm (G^m)^{-1} \right\}. \quad (40)$$

3.3. Periodicity condition

The cell function χ is Q -periodic, i.e., it satisfies:

$$\chi^m(y_1 + L_1, y_2) = \chi^m(y_1, y_2) = \chi^m(y_1 + L_2 \cos \varphi, y_2 + L_2 \sin \varphi). \quad (41)$$

This periodicity requirement is enforced by identifying the representation (30) valid in the matrix domain with a linear combination of doubly-periodic basis functions defined in terms of the complex variable

$$z = \frac{y_1 + iy_2}{L_1} = \frac{re^{i\theta}}{L_1} = \hat{R} \rho e^{i\theta}, \quad (42)$$

where $\hat{R} = R/L_1$ is the dimensionless fibre radius. Accordingly, the relevant semi-periods are:

$$\omega_1 = \frac{1}{2}, \quad \omega_2 = \frac{\kappa}{2} e^{i\varphi}, \quad (43)$$

where $\kappa = L_2/L_1$ is the side ratio of the unit cell. More specifically, the following equation is implemented:

$$\chi_h^m = \sum_{s=1}^{+\infty} \sum_{l=1}^2 w_{slh} \Re[B_{sl}(z)], \quad (44)$$

where the coefficients w_{slh} are real unknowns and the functions $B_{sl}(z)$ are chosen in two different ways.

The most common approach, tracing back to the classical Rayleigh (1892) multipole expansion method (Perrins et al., 1979) relies on the theory of elliptic functions (Whittaker and Watson, 1927). Accordingly, the following choice is made (Kalamkarov, 1992; Meguid and Kalamkarov, 1994; Rodríguez-Ramos et al., 2001; Bisegna and Caselli, 2008):

$$B_{sl}(z) = \begin{cases} -\eta_l z + \omega_l \zeta(z) & \text{if } s = 1, l = 1, 2; \\ \omega_l \frac{\zeta^{(s-1)}(z)}{(s-1)!} & \text{for } s > 1, \text{ odd } s, l = 1, 2, \end{cases} \quad (45)$$

where $\zeta(z)$ denotes the Weierstrass Zeta function of semiperiods ω_1, ω_2 . It is odd and quasi-periodic, that is:

$$\zeta(z + 2\omega_k) = \zeta(z) + 2\eta_k, \quad (46)$$

with $k = 1, 2$ and $\eta_k = \zeta(\omega_k)$. The latter quantities are linked to the semiperiods ω_1, ω_2 by Legendre's relationship:

$$\eta_1 \omega_2 - \eta_2 \omega_1 = \frac{1}{2} \pi i. \quad (47)$$

Using (46) and (47), and recalling that the derivatives of $\zeta(z)$ are elliptic functions, it is easy to verify that the basis functions $\Re[B_{sl}(z)]$ are indeed doubly periodic, with semiperiods ω_1, ω_2 . Only odd functions $B_{sl}(z)$ are introduced here, due to condition (32).

In the cited literature, the unit cell is symmetric with respect to the y_1 and y_2 axes. This implies evenness or oddness properties for the cell function χ_h^m , which is consequently represented by the subset of the functions (45) corresponding to $l = 1$ or $l = 2$ only. In this work no such symmetry is assumed, and hence the whole set (45) is considered.

A different choice for the functions $B_{sl}(z)$ is also considered here, coinciding with the one proposed by Parnell and Abrahams (2006) if the geometry is rectangular, i.e., $\varphi = \pi/2$:

$$B_{sl}(z) = \begin{cases} \Phi_1(z, \omega_1, \omega_2) & \text{if } (s, l) = (1, 1); \\ \Phi_1(e^{-i\varphi}z, e^{-i\varphi}\omega_2, e^{-i\varphi}\omega_1) & \text{if } (s, l) = (1, 2); \\ \Phi_s(z, \omega_1, \omega_2) & \text{for } s > 1, \text{ odd } s, l = 1; \\ i\Phi_s(z, \omega_1, \omega_2) & \text{for } s > 1, \text{ odd } s, l = 2. \end{cases} \quad (48)$$

Here

$$\begin{aligned} \Phi_1(z, \omega_1, \omega_2) &= \frac{\pi}{2\omega_1} \cot \frac{\pi z}{2\omega_1} + \frac{\pi}{2\omega_1} \\ &\times \sum_{n=1}^{+\infty} \left[\cot \frac{\pi}{2\omega_1} (z - 2n\omega_2) + \cot \frac{\pi}{2\omega_1} (z + 2n\omega_2) \right], \end{aligned} \quad (49)$$

where the $\pm n$ terms in the sum are paired to ensure convergence (Parnell and Abrahams, 2006), and, for $s > 1$, odd s :

$$\Phi_s(z, \omega_1, \omega_2) = \left(\frac{\pi}{2\omega_1} \right)^s \sum_{n=-\infty}^{+\infty} \frac{\cos \frac{\pi}{2\omega_1} (z + 2n\omega_2)}{\sin^s \frac{\pi}{2\omega_1} (z + 2n\omega_2)}. \quad (50)$$

In the preceding as well, only odd functions $B_{sl}(z)$ are introduced, due to condition (32).

The identification of (30) and (44) is easily obtained by considering the Laurent series of each function $B_{sl}(z)$, having a pole of order s at $z = 0$, as follows:

$$B_{sl}(z) = \sum_{k=1}^s \frac{v_{ksl}}{z^k} + \sum_{k=1}^{+\infty} \zeta_{ksl} z^k, \quad (51)$$

where v_{ksl} and ζ_{ksl} are the series coefficients of the singular and regular part of $B_{sl}(z)$, respectively. The first sum at the right-hand side of (51) is extended to $+\infty$, by setting $v_{ksl} = 0$ for $k > s$. Hence, (44) is transformed into:

$$\chi_h^m = \Re \left[\sum_{k=1}^{+\infty} \left(\sum_{s=1}^{+\infty} \sum_{l=1}^2 v_{ksl} w_{slh} \right) z^{-k} + \sum_{k=1}^{+\infty} \left(\sum_{s=1}^{+\infty} \sum_{l=1}^2 \zeta_{ksl} w_{slh} \right) z^k \right], \quad (52)$$

which, recalling (42), is compared term-by-term to (30) and yields, for odd natural numbers k :

$$\hat{R}^k b_{(-k)h} = \sum_{s=1}^{+\infty} \sum_{l=1}^2 v_{ksl} w_{slh}, \quad (53)$$

$$\hat{R}^{-k} b_{kh} + L_1 c_h \delta_{k1} = \sum_{s=1}^{+\infty} \sum_{l=1}^2 \zeta_{ksl} w_{slh}. \quad (54)$$

Here δ is the Kronecker symbol, and

$$c_h = \begin{cases} 1 & \text{if } h = 1, \\ -i & \text{if } h = 2, \end{cases} \quad (55)$$

so that $y_h = \Re(c_h r e^{i\theta})$.

3.4. Solution of the cell problem and effective constitutive tensor

The solution of the cell problem is achieved by substituting (53) and (54) into the interface boundary condition (38)₂, leading to:

$$\hat{R}^k \sum_{s=1}^{+\infty} \sum_{l=1}^2 \zeta_{ksl} w_{slh} - R c_h \delta_{k1} = \gamma_k \hat{R}^{-k} \sum_{s=1}^{+\infty} \sum_{l=1}^2 \bar{v}_{ksl} w_{slh}. \quad (56)$$

Making the position (Nicorovici et al., 1993)

$$q_{slh} = \frac{\sqrt{s}}{R^s} w_{slh}, \quad (57)$$

the following infinite set of linear algebraic equations is obtained, for odd natural numbers k :

$$\sum_{s=1}^{+\infty} \sum_{l=1}^2 \sqrt{\frac{k}{s}} \left(\gamma_k \hat{R}^{s-k} \bar{v}_{ksl} - \hat{R}^{k+s} \zeta_{ksl} \right) q_{slh} = -R c_h \delta_{k1}. \quad (58)$$

Taking the real and imaginary parts of the latter allows to compute the real unknowns q_{slh} , which in turn determine w_{slh} via (57), $b_{(-k)h}$ via (53), and b_{kh} , a_{kh} via (38). Hence, the cell functions χ_h^m , χ_h^f are computed by (30) and (31).

Of course, it is necessary to truncate the system (58) to a finite order N , amounting to taking into account a finite number of coefficients in the representations (30) and (31). It is shown in Section 5 that taking N of the order of units yields satisfactory results for volume-fraction values of practical interest.

Finally, the effective material tensor $\mathbf{G}^\#$ follows from (28). After some algebra, it turns out that:

$$G_{hj}^\# = G^m \delta_{hj} + \frac{f}{R} \Re \left[G^m (\bar{c}_h b_{1j} + c_h b_{-1j}) - G^f \Psi \bar{c}_h a_{1j} \right], \quad (59)$$

with

$$\begin{aligned} \Psi &= g(1) - \int_0^1 [\rho g'(\rho) + (1 - \sigma^2)g(\rho)] W_1(\rho) d\rho \\ &= \int_0^1 g(\rho) [\rho W_1'(\rho) + \sigma^2 W_1(\rho)] d\rho. \end{aligned} \quad (60)$$

For a general grading profile, the above coefficient Ψ , as well as the coefficients $W_k'(1)$ entering (39) and (40), can be computed via numerical integration of (33)–(35). However, closed-form solutions to the latter problem for large families of grading profiles are presented in Section 4.

3.5. Weierstrass basis functions

An asset of the Weierstrassian approach (45) to the construction of the doubly-periodic basis functions $\Re[B_{sl}(z)]$ is that the coefficients v_{ksl} , ζ_{ksl} entering (51) are easily computed. Indeed, the Laurent series expansion of $\zeta(z)$ is:

$$\zeta(z) = \frac{1}{z} - \sum_{k=2}^{+\infty} c_k \frac{z^{2k-1}}{2k-1}, \quad (61)$$

where c_k , $k \geq 2$ is given by the following rapidly convergent Fourier series (Apostol, 1997):

$$\frac{c_k}{2k-1} = 2(2\omega_1)^{-2k} \left[\zeta_R(2k) + \frac{(2\pi i)^{2k}}{(2k-1)!} \sum_{n=1}^{+\infty} \sigma_{2k-1}(n) e^{2\pi i n \omega_2 / \omega_1} \right]. \quad (62)$$

Here $\zeta_R(\alpha) = \sum_{n=1}^{+\infty} n^{-\alpha}$ is the Riemann Zeta function, and $\sigma_\alpha(n) = \sum_{d|n} d^\alpha$ is the divisor function. Accordingly, the Laurent series expansion of the $(s-1)$ th derivative of $\zeta(z)$, $s \geq 1$, odd s , is:

$$\frac{\zeta^{s-1}(z)}{(s-1)!} = z^{-s} - \sum_{k=1}^{+\infty} \mu_{ks} z^k, \quad (63)$$

where for odd natural numbers k , s ,

$$\mu_{ks} = \frac{1}{k+s-1} \binom{k+s-1}{s-1} c_{\frac{k+s}{2}}. \quad (64)$$

Here round brackets denote the binomial coefficient, and it has been stipulated that $c_1 = 0$ for ease of notation. Hence, from (45), (51) and (63), it follows that:

$$v_{ksl} = \omega_l \delta_{ks}, \quad \zeta_{ksl} = -\omega_l \mu_{ks} - \eta_l \delta_{k1} \delta_{s1}. \quad (65)$$

The special structure of v_{ksl} is due to the fact that the Laurent expansion of $\zeta^{(s-1)}(z)$ has the only singular term z^{-s} , according to (63). This implies that the multipole contribution of order s comes from the basis functions $\Re[B_{s1}(z)]$ and $\Re[B_{s2}(z)]$ only: this is a very useful

feature, leading to a noteworthy simplification of the foregoing theory. In particular, (53) reduces to:

$$\hat{R}^k b_{(-k)h} = \sum_{l=1}^2 \omega_l w_{klh}, \quad (66)$$

whereas (58) reduces to:

$$\gamma_k \sum_{l=1}^2 \bar{\omega}_l q_{klh} + \sum_{s=1}^{+\infty} S_{ks} \sum_{l=1}^2 \omega_l q_{slh} + \delta_{k1} \hat{R}^2 \sum_{l=1}^2 \eta_l q_{1lh} = -R c_h \delta_{k1}, \quad (67)$$

where $S_{ks} = \mu_{ks} \hat{R}^{k+s} \sqrt{k/s}$ turns out to be a symmetric matrix (Nicorovici et al., 1993). Then, substituting (38), (66) and (57) into (59), the following expression for the effective material tensor is obtained:

$$\mathbf{G}^\# = \mathbf{G}^m \mathbf{I} - f[(1 + \gamma_1^{-1}) \mathbf{G}^m - \Psi \lambda_1 \gamma_1^{-1} \mathbf{G}^r] \mathbf{H}, \quad (68)$$

where the tensor \mathbf{H} is defined by:

$$H_{hj} = -\frac{\gamma_1}{R} \sum_{l=1}^2 \Re(c_h \omega_l) q_{1lj}. \quad (69)$$

Simple closed-form formulas for \mathbf{H} , and hence for $\mathbf{G}^\#$, are obtained by truncating the infinite system (67) to the order $N = 1$ or 2 . In particular, for $N = 1$ it follows that:

$$\mathbf{H} = \frac{\mathbf{I} + \frac{2f}{\gamma_1} \mathbf{U} + \frac{p_1 f}{\gamma_1} \mathbf{\Lambda}_{\eta_1}}{1 + \frac{2f}{\gamma_1} + \frac{p_2 f^2}{\gamma_1^2}}, \quad (70)$$

whereas for $N = 2$ it turns out that:

$$\mathbf{H} = \frac{\left(1 - \frac{p_3 f^4}{\gamma_1 \gamma_3} - \frac{p_4 f^6}{\gamma_1^2 \gamma_3}\right) \mathbf{I} + \left(\frac{2f}{\gamma_1} - \frac{2p_4 f^7}{\gamma_1 \gamma_3}\right) \mathbf{U} + \left(\frac{p_1 f}{\gamma_1} - \frac{2p_5 f^7}{\gamma_1 \gamma_3}\right) \mathbf{\Lambda}_{\eta_1} + \frac{p_6 f^7}{\gamma_1 \gamma_3} \mathbf{\Lambda}_{\mu_{13}^2 \mu_{33}}}{1 + \frac{2f}{\gamma_1} + \frac{p_2 f^2}{\gamma_1^2} - \frac{2p_3 f^4}{\gamma_1 \gamma_3} - \frac{2p_4 f^6}{\gamma_1^2 \gamma_3} - \frac{2p_5 f^7}{\gamma_1 \gamma_3} + \frac{p_7 f^8}{\gamma_1^2 \gamma_3}}. \quad (71)$$

In (70) and (71) the following positions are made:

$$\begin{aligned} p_1 &= (2/\pi) \kappa \sin \varphi, \quad p_2 = (4/\pi^2) (\pi \Re \eta_1 - |\eta_1|^2 \kappa \sin \varphi) \kappa \sin \varphi, \\ p_3 &= |\mu_{13}|^2 (\kappa \sin \varphi)^4 / (3\pi^4), \quad p_4 = |\mu_{33}|^2 (\kappa \sin \varphi)^6 / \pi^6, \\ p_5 &= |\mu_{33}|^2 (\kappa \sin \varphi)^7 / \pi^7, \quad p_6 = (\kappa \sin \varphi)^7 / (3\pi^7), \\ p_7 &= [|\mu_{13}|^4 + 36|\eta_1|^2 |\mu_{33}|^2 - 12\Re(\mu_{13}^2 \bar{\mu}_{33} \bar{\eta}_1)] (\kappa \sin \varphi)^8 / (9\pi^8) \\ &\quad + 2[\Re(\mu_{13}^2 \bar{\mu}_{33}) - 6|\mu_{33}|^2 \Re \eta_1] (\kappa \sin \varphi)^7 / (3\pi^7), \end{aligned} \quad (72)$$

and, for a complex number q with real and imaginary parts $\Re q$ and $\Im q$, respectively,

$$\mathbf{\Lambda}_q = \begin{pmatrix} -\Re q & \Im q \\ \Im q & \Re q \end{pmatrix}, \quad \mathbf{U} = \begin{pmatrix} 1 & 0 \\ 0 & 0 \end{pmatrix}. \quad (73)$$

It is pointed out that the quantities p_1, \dots, p_7 and the tensors $\mathbf{\Lambda}_{\eta_1}$, $\mathbf{\Lambda}_{\mu_{13}^2 \mu_{33}}$ depend on the geometry of the unit cell only, i.e., on κ and φ . Indeed, η_1 and μ_{ks} are easily computed as functions of the latter quantities, as recalled above. The material properties enter Eqs. (71) and (68) through the quantities γ_k , λ_1 , \mathbf{G}^m , \mathbf{G}^r , Ψ . The dependence on the volume fraction f is explicitly traced.

The range of validity of the expressions (70) and (71) is ascertained in Section 5.

3.5.1. Special fibre arrangements

The fibre arrangement considered herein (Fig. 1) is centre symmetric with respect to the origin O , so that the cell function χ satisfies (32). For special choices of the microstructural parameters κ and φ , the fibre arrangement shares two axes of orthogonal symmetry, a feature which greatly simplifies the analysis. It is easy to verify that such choices include:

- $\varphi = \pi/2$ and any κ (rectangular unit cell), or
- $\kappa = 1$ and any φ (rhombic unit cell), or
- $2\kappa \cos \varphi$ is an integer number, or
- $2\kappa^{-1} \cos \varphi$ is an integer number.

The most interesting situation for applications is the first one, which is briefly considered in this section.

Assuming $\varphi = \pi/2$ implies that ω_1 , η_1 and the coefficients μ_{ks} are real, whereas ω_2 , η_2 are purely imaginary (Abramowitz and Stegun, 1965). Consequently, Eq. (67) yields two uncoupled systems. In particular, the real [respectively, imaginary] part of (67) involves the unknowns q_{k1h} [respectively, q_{k2h}], and yields $q_{k12} = 0$ [respectively, $q_{k21} = 0$], so that, according to (68) and (69), the tensors \mathbf{H} and $\mathbf{G}^\#$ turn out to be diagonal, as expected. Moreover, (67) is simplified into:

$$\left(\mathbf{I} + \frac{\hat{R}^2 \eta_h}{\gamma_1 \bar{\omega}_h} \mathbf{u} \otimes \mathbf{u} + (-1)^{h-1} \mathbf{S} \mathbf{\Gamma}^{-1} \right) \mathbf{\Gamma} \mathbf{q} = -\frac{R c_h}{\bar{\omega}_h} \mathbf{u}, \quad (74)$$

for $h = 1, 2$, where the unknowns q_{khh} , odd k , have been arranged into a vector \mathbf{q} , \mathbf{I} is the identity matrix, the vector \mathbf{u} has the only nonzero element $u_1 = 1$, $\mathbf{\Gamma}$ is a diagonal matrix having diagonal entries γ_k defined in (39), and \mathbf{S} is the symmetric matrix with entries S_{ks} . By truncating the infinite system (74) to a finite order N , and applying Cramer's rule and standard properties of determinants, it turns out that:

$$-\frac{2\eta_h R}{c_h L_1^2} q_{1hh} = 1 - \frac{\det \left[\mathbf{I} - \frac{\hat{R}^2 \eta_h}{\gamma_1 \bar{\omega}_h} \mathbf{u} \otimes \mathbf{u} + (-1)^{h-1} \mathbf{S} \mathbf{\Gamma}^{-1} \right]}{\det \left[\mathbf{I} + \frac{\hat{R}^2 \eta_h}{\gamma_1 \bar{\omega}_h} \mathbf{u} \otimes \mathbf{u} + (-1)^{h-1} \mathbf{S} \mathbf{\Gamma}^{-1} \right]} \Big|_N, \quad (75)$$

where \det denotes the determinant and the suffix N denotes the truncation to the order N . Then, recalling (69) and the definitions of \mathbf{S} , $\mathbf{\Gamma}$, \mathbf{u} , and expanding the determinants appearing in (75) (Bisegna and Caselli, 2008, Appendix B), the following closed-form expression for H_{hh} , $h = 1, 2$, to any truncation order N is obtained:

$$\frac{2(-1)^{h-1} \kappa \eta_h f}{\pi \omega_h \gamma_1} H_{hh} = 1 - \frac{\gamma_1^- \sum_{n=0}^N \sum_{l \in N \setminus \mathcal{C}_n} (\det \mathbf{M}_{l,l}) \left(\frac{(-1)^{h-1} \kappa f}{\pi} \right)^{|l|} \prod_{k \in l} (\gamma_k^-)^{-1}}{\gamma_1^+ \sum_{n=0}^N \sum_{l \in N \setminus \mathcal{C}_n} (\det \mathbf{M}_{l,l}) \left(\frac{(-1)^{h-1} \kappa f}{\pi} \right)^{|l|} \prod_{k \in l} (\gamma_k^+)^{-1}}. \quad (76)$$

Here $\gamma_k^\pm = \gamma_k$, odd k , with the exception of $\gamma_1^\pm = \gamma_1 \pm \hat{R}^2 \eta_h / \bar{\omega}_h = \gamma_1 \pm (-1)^{h-1} \kappa \eta_h f / (\pi \omega_h)$; $N \setminus \mathcal{C}_n$ is the set of the combinations of the N odd indices $\{1, 3, \dots, 2N-1\}$ taken n at a time; \mathbf{M} is the matrix with elements μ_{ks} defined in (64), for odd k, s ; $\mathbf{M}_{l,l}$ is the principal minor of \mathbf{M} corresponding to the rows and the columns with index in the subset l ; finally, $|l|$ is the sum of the elements of l . It is stipulated that $\det \mathbf{M}_{l,l} = 1$ and $\prod_{k \in l} (\gamma_k^\pm)^{-1} = 1$, if l is the empty set. The values of η_h , μ_{ks} can be calculated as recalled in Section 3.5, or Table 18.3 of Abramowitz and Stegun (1965).

The formula obtained by taking $N = 1$ [respectively, 2] in (76) coincides with (70) [respectively, (71)], when $\varphi = \pi/2$ is enforced in the latter. On the other hand, (76) reduces to well-known formulas for square fibre arrangements, when $\kappa = 1$ and small values of N are taken (Rayleigh, 1892; Perrins et al., 1979; Gu and Liu, 1992). To the authors' knowledge, the closed-form formulas (70) and (71) for general fibre arrangements, and expression (76) for rectangular fibre arrangements, are presented here for the first time.

4. Fibre grading profiles

In this section, closed-form solutions W_k of Problem (33)–(35) are derived for different grading profiles $g(\rho)$.

4.1. Homogeneous fibres

For homogeneous cylindrically-orthotropic fibres, i.e., $g(\rho) = 1$, Eqs. (33)–(35) imply

$$W_k(\rho) = \rho^{\sigma k}, \quad (77)$$

so that $W'_k(1) = \sigma k$ and $\Psi = \sigma$. If, moreover, fibres are transversely-isotropic (i.e., $G^r = G^\theta$, viz. $\sigma = 1$), it turns out that $W'_k(1) = k$, $\Psi = 1$ (Perrins et al., 1979; Gu and Liu, 1992; Rodríguez-Ramos et al., 2001).

4.2. Exponentially-graded fibres

The grading function

$$g(\rho) = \exp(-\lambda \rho^q), \quad (78)$$

with λ and $q > 0$ material parameters, is considered. It was studied by Martin (2002) with reference to spherical inclusions. The particular case $q = 1$ was treated in Chen and Kuo (2005) and Wei et al. (2006).

Substituting (78) in (33) gives

$$W''_k + \left(\frac{1 - \lambda q \rho^q}{\rho} \right) W'_k - \frac{\sigma^2 k^2}{\rho^2} W_k = 0. \quad (79)$$

Introducing the change of variables

$$z = \lambda \rho^q, \quad w_k = \rho^{-\sigma k} W_k, \quad (80)$$

Kummer's differential equation is obtained (Abramowitz and Stegun, 1965):

$$z w''_k + (b_k - z) w'_k - a_k w_k = 0, \quad (81)$$

where

$$a_k = \frac{\sigma k}{q}, \quad b_k = 1 + \frac{2\sigma k}{q}. \quad (82)$$

Hence, recalling (34) and (80), it follows that (Abramowitz and Stegun, 1965):

$$W_k(\rho) = \rho^{\sigma k} \frac{{}_1F_1(a; b; \lambda \rho^q)}{{}_1F_1(a; b; \lambda)}. \quad (83)$$

Here ${}_1F_1$ is Kummer's function, defined by:

$${}_1F_1(a; b; z) = \sum_{n=0}^{+\infty} \frac{(a)_n}{(b)_n} \frac{z^n}{n!}, \quad (84)$$

provided that b is not a nonnegative integer, and the Pochhammer symbol $(a)_n$ is given by

$$(a)_n = \frac{\Gamma(a+n)}{\Gamma(a)}, \quad (a)_0 = 1, \quad (85)$$

where Γ denotes the Gamma function. Using the differentiation formula for ${}_1F_1$ (Abramowitz and Stegun, 1965), it follows that:

$$W'_k(1) = \sigma k + q \lambda \frac{a}{b} \frac{{}_1F_1(a+1; b+1; \lambda)}{{}_1F_1(a; b; \lambda)}. \quad (86)$$

The factor Ψ can be computed from (60) via numerical quadrature.

4.3. Special-function graded fibres

New wide classes of grading functions allowing closed-form solutions are derived in this section. Setting

$$W_k(\rho) = \frac{w_k(\rho)}{h(\rho)}, \quad (87)$$

with $h(\rho)$ a function to be chosen, transforms (33) into:

$$w''_k + \left(\frac{1}{\rho} + \frac{g'}{g} - \frac{2h'}{h} \right) w'_k + \left[-\frac{h''}{h} - \frac{h'}{h} \left(\frac{1}{\rho} + \frac{g'}{g} - \frac{2h'}{h} \right) - \frac{\sigma^2 k^2}{\rho^2} \right] w_k = 0. \quad (88)$$

If h is chosen such that $h = \sqrt{g}$, then it turns out that $g'/g - 2h'/h = 0$, and the above equation simplifies into:

$$w''_k + \frac{1}{\rho} w'_k + \left(-\frac{h''}{h} - \frac{1}{\rho} \frac{h'}{h} - \frac{\sigma^2 k^2}{\rho^2} \right) w_k = 0. \quad (89)$$

Hence, if h solves the equation:

$$h'' + \frac{1}{\rho} h' + Hh = 0, \quad (90)$$

where $H(\rho)$ is a function to be chosen, then w_k solves the equation:

$$w''_k + \frac{1}{\rho} w'_k + \left(H - \frac{\sigma^2 k^2}{\rho^2} \right) w_k = 0. \quad (91)$$

The goal is then to select H such that both (90) and (91) admit closed-form solutions. Surprisingly simple and elegant choices are presented below.

4.3.1. Squared-Bessel graded fibres

Eqs. (90) and (91) reduce to classical Bessel equations, up to a scaling of the independent variable, when

$$H = \lambda^2 - \frac{\nu^2}{\rho^2}, \quad (92)$$

where $\lambda > 0$ and $\nu \geq 0$ are arbitrary constants. Hence, the functions h and w_k introduced above turn out to be Bessel functions. Consequently, it follows that the grading function:

$$g = J_\nu^2(\lambda \rho), \quad \left[\text{respectively, } g = Y_\nu^2(\lambda \rho) \right], \quad (93)$$

where J_ν [respectively, Y_ν] is the first-kind [respectively, second-kind] Bessel function, yields the closed-form solution:

$$W_k = \frac{J_\nu(\lambda)}{J_{\nu_k}(\lambda)} \frac{J_{\nu_k}(\lambda \rho)}{J_{\nu_k}(\lambda \rho)}, \quad \left[\text{respectively, } W_k = \frac{Y_\nu(\lambda)}{Y_{\nu_k}(\lambda)} \frac{Y_{\nu_k}(\lambda \rho)}{Y_{\nu_k}(\lambda \rho)} \right], \quad (94)$$

where $\nu_k = \sqrt{\nu^2 + \sigma^2 k^2}$. It satisfies both the regularity requirement (34) and the normalization condition (35). The quantity $W'_k(1)$ entering (39) turns out to be:

$$W'_k(1) = (\nu_k - \nu) - \lambda \left[\frac{J_{\nu_k+1}(\lambda)}{J_{\nu_k}(\lambda)} - \frac{J_{\nu+1}(\lambda)}{J_\nu(\lambda)} \right], \quad (95)$$

for the first choice in (93); the same expression, up to replacing J_ν and $J_{\nu+1}$ with Y_ν and $Y_{\nu+1}$, respectively, holds for the second choice. It is pointed out that the latter implies unbounded values of the material elastic shear moduli near the fibre axis.

It follows from (93) that the constant λ must be less than the first positive zero of J_ν [or Y_ν], for the antiplane shear problem to be well posed, according to (7). In passing, it is noted that, choosing $H = -\lambda^2 - \nu^2/\rho^2$ instead of (92) leads to a grading profile in the form of a squared modified Bessel function of first or second kind, i.e., $I_\nu^2(\lambda \rho)$ or $K_\nu^2(\lambda \rho)$.

To the best of the authors' knowledge, the solutions presented in this Section are new.

4.3.2. Squared-hypergeometric graded fibres

A very broad class of grading functions yielding closed-form solutions are obtained by resorting to the theory of Gaussian hypergeometric functions. Indeed, Riemann's form of the general-

ized hypergeometric equation with (regular) singular points $0, \infty, 1$ is (Abramowitz and Stegun, 1965):

$$u'' + \left(\frac{1 - \alpha - \alpha'}{z} - \frac{1 - \gamma - \gamma'}{1 - z} \right) u' + \left(\frac{\alpha\alpha'}{z} + \frac{\gamma\gamma'}{1 - z} - \beta\beta' \right) \frac{u}{z(1 - z)} = 0, \quad (96)$$

where (α, α') , (β, β') and (γ, γ') are the respective pairs of the exponents, linked by the relation:

$$\alpha + \alpha' + \beta + \beta' + \gamma + \gamma' = 1. \quad (97)$$

Eq. (96) admits the solution:

$$u = z^\alpha (1 - z)^\gamma {}_2F_1(\alpha + \beta + \gamma, \alpha + \beta' + \gamma; 1 + \alpha - \alpha'; z), \quad (98)$$

where ${}_2F_1$ is the hypergeometric function, which can be computed, e.g., via the Gauss hypergeometric series, absolutely convergent in $\{|z| < 1\}$:

$${}_2F_1(a, b; c; z) = \sum_{n=0}^{+\infty} \frac{(a)_n (b)_n}{(c)_n} \frac{z^n}{n!} \quad (99)$$

provided that c is not a nonnegative integer, with the Pochhammer symbol defined in (85).

Choosing $\alpha + \alpha' = 0$, $\gamma + \gamma' = 1$, and hence $\beta + \beta' = 0$ by (97), makes the first two terms on the left-hand side of (96) coincide with the corresponding terms of (90) and (91). This suggests that, with a suitable choice of H , (90) can be formally reduced to (96). Indeed, up to the scaling $\rho = z/\lambda$ of the independent variable, this is the case by choosing:

$$H = \left(-\frac{\alpha^2}{\lambda\rho} + \frac{\gamma(1-\gamma)}{1-\lambda\rho} + \beta^2 \right) \frac{\lambda^2}{\lambda\rho(1-\lambda\rho)}, \quad (100)$$

where α, β, γ and λ are arbitrary constants. More interesting than that, even (91) can be formally reduced to (96), since it turns out that:

$$H - \frac{\sigma^2 k^2}{\rho^2} = \left(-\frac{\alpha_k^2}{\lambda\rho} + \frac{\gamma(1-\gamma)}{1-\lambda\rho} + \beta_k^2 \right) \frac{\lambda^2}{\lambda\rho(1-\lambda\rho)}, \quad (101)$$

where

$$\alpha_k = \pm \sqrt{\alpha^2 + \sigma^2 k^2}, \quad \beta_k = \pm \sqrt{\beta^2 + \sigma^2 k^2}. \quad (102)$$

Hence, it follows that:

$$h = (\lambda\rho)^\alpha (1 - \lambda\rho)^\gamma {}_2F_1(\alpha + \beta + \gamma, \alpha - \beta + \gamma; 1 + 2\alpha; \lambda\rho), \quad (103)$$

$$w_k = (\lambda\rho)^{\alpha_k} (1 - \lambda\rho)^\gamma {}_2F_1(\alpha_k + \beta_k + \gamma, \alpha_k - \beta_k + \gamma; 1 + 2\alpha_k; \lambda\rho). \quad (104)$$

Consequently, for any grading $g = h^2$ parameterized by the four arbitrary constants α, β, γ and λ appearing in (103), the closed-form solution $W_k = Cw_k/h$ is obtained. The regularity requirement (34) and the normalization condition (35) can be, respectively, satisfied by a suitable choice of the signs in (102) and of the multiplicative constant C . The following noteworthy examples, some of which are new in the literature, will help clarifying this point.

4.3.2.1. Power-law graded fibres. Choosing $\beta = \alpha$, $\gamma = 0$ and $\lambda = 1$, with arbitrary α , the following grading is obtained:

$$g(\rho) = \rho^{2\alpha}, \quad (105)$$

which yields the closed-form solution:

$$W_k = \rho^{\alpha_k - \alpha}, \quad (106)$$

with $\alpha_k = \sqrt{\alpha^2 + \sigma^2 k^2}$. Hence,

$$W'_k(1) = \alpha_k - \alpha, \quad \Psi = \frac{\sigma^2 + \alpha_1 - \alpha}{1 + \alpha_1 + \alpha}. \quad (107)$$

If $\alpha = 0$, the values for homogeneous fibres (Section 4.1) are recovered. It is noted that, with the grading (105), (33) becomes an Euler equation, directly yielding (106). This grading profile has been repeatedly considered in the literature (e.g., Gu and Yu, 2003).

4.3.2.2. Binomial-power-law graded fibres. The choice $\alpha = 0$, $\beta = \gamma = v/2$ with arbitrary v leads to:

$$g(\rho) = (1 - \lambda\rho)^v. \quad (108)$$

The parameter λ is assumed to be less than 1, so that g does not vanish for $\rho \in [0, 1]$. The case $\lambda = 0$ implies homogeneous fibres. If $0 < \lambda < 1$, the following closed-form solution is obtained:

$$W_k(\rho) = C(\lambda\rho)^{\alpha_k} {}_2F_1(\alpha_k + \beta_k + \gamma, \alpha_k - \beta_k + \gamma; 1 + 2\alpha_k; \lambda\rho), \quad (109)$$

with $\alpha_k = \sigma k$, $\beta_k = \sqrt{v^2/4 + \sigma^2 k^2}$, and C chosen in order to fulfill the normalization condition (35). The factor $W'_k(1)$ can be computed using the differentiation formula for ${}_2F_1$ (Abramowitz and Stegun, 1965).

If $\lambda < 0$, $\lambda\rho$ is negative for $\rho \in [0, 1]$, and its modulus need not be upper bounded by 1. Hence, the representation (99) may not converge. The following Bolza's formula (Abramowitz and Stegun, 1965) is employed instead:

$${}_2F_1(a, b; c; z) = (1 - z)^{-a} {}_2F_1\left(a, c - b; c; \frac{z}{z - 1}\right). \quad (110)$$

In fact, the right-hand side of (110) converges for $\{\Re z < \frac{1}{2}\}$ when computed via (99) (Tricomi, 1965). Hence, from (109) and (110), it follows that:

$$W_k(\rho) = C(1 - \lambda\rho)^{-\beta_k - \gamma} \left(\frac{-\lambda\rho}{1 - \lambda\rho} \right)^{\alpha_k} \cdot {}_2F_1\left(\alpha_k + \beta_k + \gamma, 1 + \alpha_k + \beta_k - \gamma; 1 + 2\alpha_k; \frac{-\lambda\rho}{1 - \lambda\rho}\right). \quad (111)$$

As in the previous case, the constant C is chosen in order to fulfill the normalization condition (35), and the factor $W'_k(1)$ is computed similarly.

The grading profile (108) was considered by Gu and Yu (2003), in the particular case $v = 1$. In turn, when $\lambda < 0$, it is a particular case of the grading profile treated in Wei et al. (2006) by power series.

4.3.2.3. New families of grading profiles allowing closed-form solutions. Many more solutions can be generated by (103) and (104). As an example, choosing α, β, γ such that $\alpha + \beta + \gamma$ or $\alpha - \beta + \gamma$ is a negative integer $-n$, the hypergeometric series (99) stops to its n th term, reducing to a polynomial. In particular,

- choosing $\alpha = -\frac{1}{4}$, $\beta = -n$, $\gamma = \frac{1}{4}$, and recalling that ${}_2F_1(-n, n; \frac{1}{2}; x) = T_n(1 - 2x)$, it follows that the grading $g(\rho) = (\lambda\rho)^{-\frac{1}{2}} (1 - \lambda\rho)^{\frac{1}{2}} T_n^2(1 - 2\lambda\rho)$, where T_n denotes the Chebyshev polynomial of order n , yields the closed-form solution:

$$W_k(\rho) = C \frac{(\lambda\rho)^{\alpha_k + \frac{1}{4}} {}_2F_1(\alpha_k + \beta_k + \gamma, \alpha_k - \beta_k + \gamma; 1 + 2\alpha_k; \lambda\rho)}{T_n(1 - 2\lambda\rho)}; \quad (112)$$

- choosing $\alpha = 0$, $\beta = -n - \frac{1}{2}$, $\gamma = \frac{1}{2}$, and recalling that ${}_2F_1(-n, n + 1; 1; x) = P_n(1 - 2x)$, it follows that the grading $g(\rho) = (1 - \lambda\rho) P_n^2(1 - 2\lambda\rho)$, where P_n denotes Legendre's polynomial of order n , yields the closed-form solution:

$$W_k(\rho) = C \frac{(\lambda\rho)^{\sigma k} {}_2F_1(\sigma k + \beta_k + \frac{1}{2}, \sigma k - \beta_k + \frac{1}{2}; 1 + 2\sigma k; \lambda\rho)}{P_n(1 - 2\lambda\rho)}. \quad (113)$$

Analogous results involving Gegenbauer's polynomials $C_n^{(\alpha)}$ and Jacobi's polynomials $P_n^{(\alpha, \beta)}$ can be easily derived, recalling that ${}_2F_1(-n, n+2\alpha; \alpha+\frac{1}{2}; x) = n!C_n^{(\alpha)}(1-2x)/(2\alpha)_n$, and ${}_2F_1(-n, \alpha+1+\beta+n; \alpha+1; x) = n!P_n^{(\alpha, \beta)}(1-2x)/(\alpha+1)_n$, respectively (Abramowitz and Stegun, 1965). In these equations, $\alpha_k = \sqrt{\alpha^2 + \sigma^2 k^2}$, $\beta_k = \sqrt{\beta^2 + \sigma^2 k^2}$ and C is chosen in order to fulfill the normalization condition (35). The parameter λ must be chosen such that $g(\rho) > 0$ in $(0, 1]$, according to (7).

Moreover, exploiting the special elementary cases of Gauss series (99), closed-form solutions for W_k are obtained with other elementary grading profiles, including, e.g., the following:

- choosing $\alpha = \gamma = \frac{1}{2}$, $\beta = 0$, and recalling that ${}_2F_1(1, 1; 2; x) = -x^{-1} \log(1-x)$, it follows that the grading $g(\rho) = (\lambda\rho)^{-1} (1-\lambda\rho) \log^2(1-\lambda\rho)$, yields the closed-form solution:

$$W_k(\rho) = C \frac{(\lambda\rho)^{\alpha_k + \frac{1}{2}} {}_2F_1(\alpha_k + \sigma k + \frac{1}{2}, \alpha_k - \sigma k + \frac{1}{2}; 1 + 2\alpha_k; \lambda\rho)}{-\log(1-\lambda\rho)}; \quad (114)$$

- choosing $\alpha = \gamma = \frac{1}{4}$, $\beta = 0$, and recalling that ${}_2F_1(\frac{1}{2}, \frac{1}{2}; \frac{3}{2}; x^2) = x^{-1} \arcsin x$, it follows that the grading $g(\rho) = (\lambda\rho)^{-\frac{1}{2}} (1-\lambda\rho)^{\frac{1}{2}} \arcsin^2(\sqrt{\lambda\rho})$, yields the closed-form solution:

$$W_k(\rho) = C \frac{(\lambda\rho)^{\alpha_k + \frac{1}{4}} {}_2F_1(\alpha_k + \sigma k + \frac{1}{4}, \alpha_k - \sigma k + \frac{1}{4}; 1 + 2\alpha_k; \lambda\rho)}{\arcsin(\sqrt{\lambda\rho})}. \quad (115)$$

Other special elementary cases of Gauss series can be found in Abramowitz and Stegun (1965).

It is pointed out that the previous examples are only chosen for illustrative purposes: any grading profile $g(\rho) = h^2(\rho)$, for $h(\rho)$ given in (103) with any choice of the constants $\alpha, \beta, \gamma, \lambda$ satisfying (7), receives its closed-form solution $W_k(\rho) = w_k(\rho)/h(\rho)$ according to (87), where $w_k(\rho)$ is given by (104). To the best of the authors' knowledge, these solutions appear here for the first time.

5. Numerical results and discussion

This section is dedicated to validating the present analytical procedure and to discussing the influence of geometrical and material parameters on the overall material behaviour; attention is focused on the issue of evaluating and mitigating the shear stress in the fibre, in the matrix and at the fibre-matrix interface.

The analysis is developed by using the dimensionless parameters φ , $\kappa = L_2/L_1$, $f = \pi R^2/|Q|$, $\sigma^2 = G^0/G^r$ previously introduced, and the following ones:

- fibre/matrix stiffness ratio (contrast factor) $\xi = G^r/G^m$;
- grading intensity factor $\omega = g(0)/g(1)$;
- dimensionless interface parameter $\delta = D/(G^m L_1)$.

The simulations in Sections 5.1 and 5.3 refer to isotropic exponentially-graded fibres: in particular, $\sigma = 1$ and $g(\rho)$ follows (78) with $q = 1$. Consequently, it turns out that $g(0) = 1$, and $G^r = G^0$ has the meaning of shear modulus at the fibre axis. Different grading profiles $g(\rho)$ are considered in Section 5.4.

5.1. Convergence, accuracy and validation

As it was anticipated in Section 3.4, the infinite system (58), reducing to (67) in the case of Weierstrass basis functions, needs to be truncated to a finite order N . Here it is ascertained how fast convergence is achieved with respect to N , and which value of N is required to give the effective shear moduli to some chosen relative accuracy.

Reference is made to a regular hexagonal arrangement, for different values of the volume fraction. Fig. 2(a) shows that the proposed analytical scheme exhibits an exponential asymptotic rate of convergence, which turns out to be faster for lower volume fraction values.

Table 1 shows the minimum value of N required for the effective shear modulus $G^\#$ to have a relative accuracy of 10^{-2} , 10^{-4} or 10^{-6} , respectively. This value increases with volume fraction f and with fibre/matrix contrast factor ξ (Perrins et al., 1979). A value of N of few units will suffice in most cases of practical interest. Other simulations, not shown for conciseness, indicate that even lower N values are required in the case of

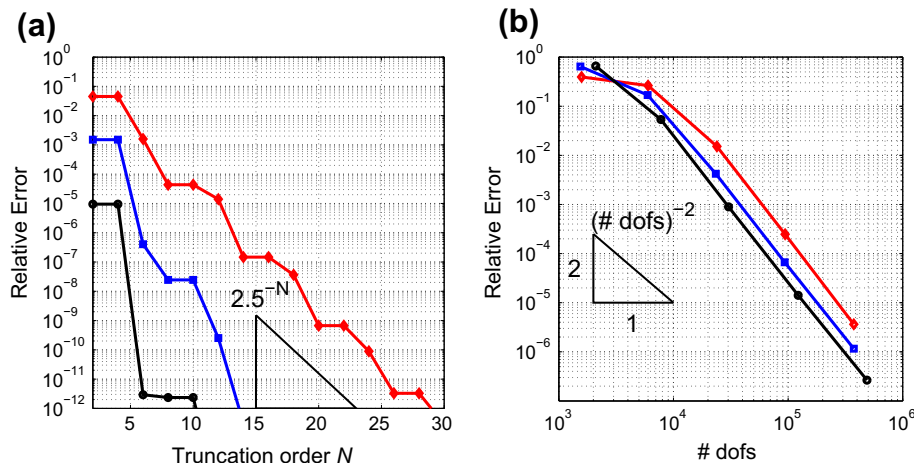


Fig. 2. (a) Convergence property of the present approach: relative error on effective modulus $G^\#$ versus truncation order N . Overkill solution: present approach, $N = 100$. (b) Convergence of FEM solution to present solution ($N = 100$): relative error on effective modulus $G^\#$ versus number of FEM degrees of freedom. Cell geometry: $\kappa = 1$, $\varphi = \pi/3$; $f = 0.25$ – black circles, $f = 0.5$ – blue squares, $f = 0.75$ – red diamonds. Material parameters: $\xi = 500$, $\sigma = 1$, $\delta = +\infty$. Grading type: exponential; grading intensity $\omega = 4$. (For interpretation of the references to color in this figure legend, the reader is referred to the web version of this paper.)

Table 1

Present analytical solution. Regular hexagonal cell with exponentially-graded isotropic fibres, $\omega = 4$, $\sigma = 1$, and perfect interface, $\delta = +\infty$. Minimum order N required to give the effective shear modulus to the relative accuracy R of 10^{-2} , 10^{-4} and 10^{-6} . N is listed for various values of the volume fraction f and of the material shear moduli contrast factor ξ .

| | $R = 10^{-2}$ | | | $R = 10^{-4}$ | | | $R = 10^{-6}$ | | |
|-----|---------------|----|-----|---------------|----|-----|---------------|----|-----|
| | ξ | | | ξ | | | ξ | | |
| f | 5 | 50 | 500 | 5 | 50 | 500 | 5 | 50 | 500 |
| 0.1 | 1 | 1 | 1 | 1 | 1 | 1 | 1 | 1 | 1 |
| 0.2 | 1 | 1 | 1 | 1 | 1 | 1 | 1 | 3 | 3 |
| 0.3 | 1 | 1 | 1 | 1 | 1 | 1 | 1 | 3 | 3 |
| 0.4 | 1 | 1 | 1 | 1 | 3 | 3 | 3 | 3 | 3 |
| 0.5 | 1 | 1 | 1 | 1 | 3 | 3 | 3 | 3 | 3 |
| 0.6 | 1 | 1 | 1 | 1 | 3 | 3 | 3 | 4 | 4 |
| 0.7 | 1 | 3 | 3 | 3 | 4 | 4 | 3 | 6 | 7 |
| 0.8 | 1 | 3 | 3 | 3 | 6 | 7 | 4 | 9 | 9 |
| 0.9 | 1 | 7 | 12 | 3 | 15 | 24 | 6 | 25 | 37 |

imperfect interfaces, which indeed mitigate the fibre/matrix stiffness contrast factor.

Computations were performed by using either the Weierstrass basis functions (45) or the Parnell and Abrahams (2006) type basis functions (48). In the former case, the series coefficients v_{ksl} and ξ_{ksl} of the singular and regular part of $B_{sl}(z)$ were computed using (62), (64) and (65). In the latter case, a numerical procedure to compute these coefficients was developed and coded. The sums in (49) and (50), ensuring the periodicity with respect to ω_2 , were truncated to $n = \pm 8$, yielding satisfactory results. Indeed, identical results, up to numerical round-off errors, were obtained for both choices of basis functions. This is algebraically sound, since each elliptic function $\Phi_s(z)$ appearing in (50) can be represented as a linear combination of the Weierstrass $\zeta(z)$ function and its derivatives up to the order $s - 1$ (Tricomi, 1965), i.e., of the functions defining the Weierstrass basis (45).

Beyond convergence issues, validation of the present analytical approach is obtained by comparison with a standard finite-element solution. Numerical results are obtained using the Comsol Multiphysics® 3.5 software (COMSOL AB, 2008), which easily allows to prescribe periodic boundary conditions on the unit-cell boundary.

Table 2

Dimensionless principal effective moduli ($G_h^\# / G^m$, $h = 1, 2$) for a composite with exponentially-graded isotropic fibres ($\omega = 4$, $\sigma = 1$), perfect interface ($\delta = +\infty$), contrast factor $\xi = 50$, and volume fraction $f = 0.5$. Rhombic geometry: $\kappa = 1$, $\varphi = \pi/4$ [Fig. 3(a)–(c)]. Rectangular geometry: $\kappa = 1.2$, $\varphi = \pi/2$ [Fig. 3(d)]. Analytical solution reported as a function of the truncation order N . Eqs. (68) and (69) used throughout; the latter was also substituted by a more explicit expression, when available. FEM solution based on the meshes of Fig. 3 and their repeated regular refinements. For the rhombic geometry, either a parallelogrammic [Fig. 3(a)] or a hexagonal [Fig. 3(b)] unit cell adopted. Second order Lagrangian shape functions used throughout.

| | | Rhombic geometry | | | | Rectangular geometry | |
|---------|------|---------------------|----------------|---------|------|----------------------|----------------|
| | | $G_1^\# / G^m$ | $G_2^\# / G^m$ | | | $G_1^\# / G^m$ | $G_2^\# / G^m$ |
| N | Eq. | Analytical | | N | Eq. | Analytical | |
| 1 | (70) | 2.33940115 | 3.14074837 | 1 | (76) | 3.05518877 | 2.37522191 |
| 2 | (71) | 2.35977693 | 3.21371684 | 2 | (76) | 3.15689405 | 2.41239778 |
| 4 | (69) | 2.36164973 | 3.22467809 | 4 | (76) | 3.16347567 | 2.41267851 |
| 8 | (69) | 2.36164994 | 3.22475386 | 8 | (76) | 3.16353579 | 2.41267866 |
| # dofs | | FEM (parallelogram) | | # dofs | | FEM | |
| 1219 | | 2.34786351 | 3.00293757 | 1245 | | 3.16366580 | 2.41271414 |
| 4733 | | 2.35540775 | 3.10541489 | 4865 | | 3.16354465 | 2.41268123 |
| 18,649 | | 2.35873690 | 3.17044693 | 19,233 | | 3.16353632 | 2.41267881 |
| 74,033 | | 2.36031266 | 3.19858789 | 76,481 | | 3.16353583 | 2.41267867 |
| 295,009 | | 2.36101263 | 3.21075591 | 305,025 | | 3.16353579 | 2.41267866 |
| # dofs | | FEM(hexagon) | | | | | |
| 1137 | | 2.36167607 | 3.22490495 | | | | |
| 4441 | | 2.36165171 | 3.22476374 | | | | |
| 17,553 | | 2.36165007 | 3.22475454 | | | | |
| 69,793 | | 2.36164995 | 3.22475390 | | | | |
| 278,337 | | 2.36164994 | 3.22475387 | | | | |

The first numerical test is reported in Table 2, relevant to a composite with exponentially-graded fibres ($\omega = 4$), perfect interface ($\delta = +\infty$), contrast factor $\xi = 50$, and volume fraction $f = 0.5$. Both a rhombic geometry ($\kappa = 1$, $\varphi = \pi/4$, Fig. 3(a)–(c)) and a rectangular geometry ($\kappa = 1.2$, $\varphi = \pi/2$, Fig. 3(d)) are considered. The principal effective moduli $G_h^\#$, $h = 1, 2$, i.e., the principal values of the effective tensor $\mathbf{G}^\#$, are reported, up to a scaling by G^m : due to symmetry considerations, they coincide with the components $G_{11}^\#$ and $G_{22}^\#$ of the effective stiffness tensor $\mathbf{G}^\#$ for the latter geometry, whereas they are the effective moduli along axes forming an angle of $\pi/8$ and $5\pi/8$ with the x_1 -axis, respectively, for the former geometry (Fig. 3(c)).

The analytical solution is reported as a function of the truncation order N . Eqs. (68) and (69) were used throughout. The closed-form expressions (70), (71) or (76) were also used when applicable, and yielded results identical to the ones supplied by (69). As in the previous numerical test, the same results were obtained applying the basis functions (45) or (48).

The FEM solution employed quadratic Lagrangian triangular finite elements as per meshes reported in Fig. 3(a), (b) and (d) and their regular refinements, obtained by repeatedly subdividing each triangle in four identical ones. The rhombic geometry was studied using either a parallelogrammic [Fig. 3(a)] or a hexagonal [Fig. 3(b)] unit cell: the latter supplied better results, due to the higher quality of the mesh and the greater distance of the fibre from the cell boundary. Periodicity conditions were enforced by identifying point-wise the values of the unknown cell function χ_h , $h = 1, 2$ on opposite sides of the unit cell.

As shown in Table 2, after the convergence has been reached, the same values of the principal effective moduli are supplied by the present analytical method and by the finite element method.

An even more stringent comparison is reported in Fig. 2(b). A square unit cell was considered with three different values of the fibre volume fraction and the same material parameters as in Table 2. Progressively finer meshes were considered, obtained by repeated regular refinements of an initial coarse mesh. Quadratic Lagrange triangular finite elements were employed in the analysis and the relative error on the homogenized shear modulus $G^\#$ was computed with respect to a reference solution obtained using the proposed analytical method with a very high truncation order

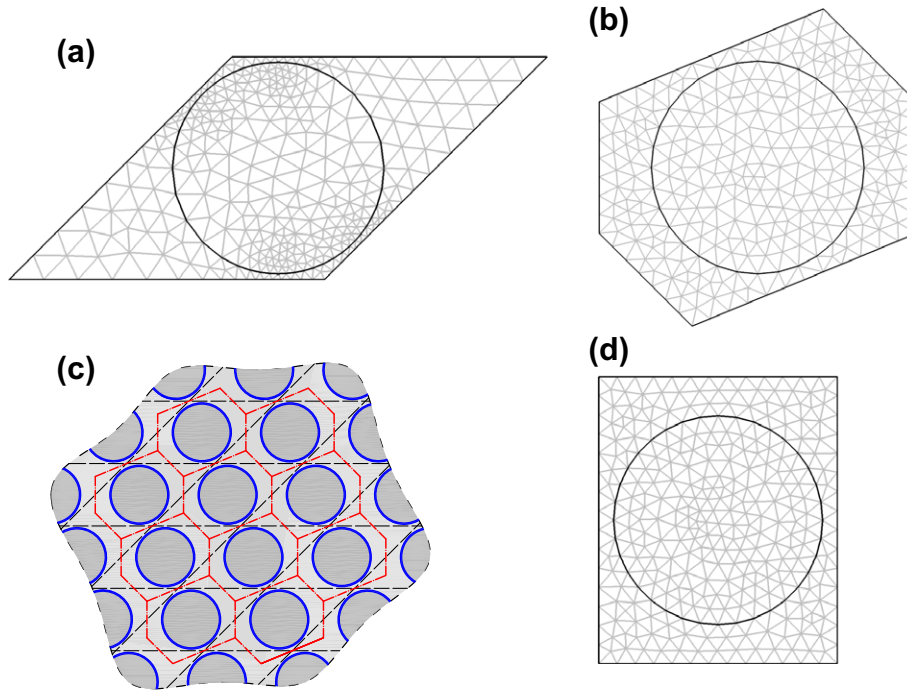


Fig. 3. FEM approach. Coarsest meshes adopted in the FEM computations of Table 2. (a)–(c) Rhombic geometry: $\kappa = 1$, $\varphi = \pi/4$, $f = 0.5$. (a) Parallelogrammic, or (b) hexagonal, unit cell; (c) corresponding lattices. (d) Rectangular geometry: $\kappa = 1.2$, $\varphi = \pi/2$, $f = 0.5$.

($N = 100$) and plotted versus the total number of degrees of freedom, in a log–log plot. The correct asymptotic convergence properties exhibited by the adopted quadratic elements shows that the FEM solution does converge to the present analytical one, thus confirming the excellent agreement obtained in Table 2. Hence, the present analytical solution procedure represents an accurate and reliable alternative to classical numerical strategies.

5.2. Comparison with other homogenization approaches

The most widely used simplified homogenization models require the computation of the concentration factor \mathbf{A}^f of a single graded fibre immersed into an unbounded matrix (e.g., Mura, 1987; Milton, 2004). This task is easily accomplished, by noting that the far shear-strain field is constant in that case: hence, the sums in (30) and (31) have to be taken over $|k| = 1$ only, and $b_{1h} = -Rc_h$, in order to have χ_h^m decaying at infinity. Then, according to (38), it turns out that $\bar{b}_{(-1)h} = -Rc_h/\gamma_1$, $a_{1h} = -Rc_h\lambda_1/\gamma_1$. Restricting the analysis to a fibre with perfect interface (i.e., $D \rightarrow +\infty$), and recalling (35), it follows that:

$$\mathbf{A}^f = \frac{1}{|Q^f|} \int_{Q^f} (\mathbf{I} - \nabla_y^t \chi) da = \frac{\lambda_1}{\gamma_1} \mathbf{I} = \frac{2}{1 + G^r g(1) W'_1(1)/G^m} \mathbf{I}. \quad (116)$$

The corresponding average shear stress in the graded fibre is obtained by applying the tensor $\mathbf{G}^{f\#} \mathbf{A}^f$, defined as follows, to the far shear-strain field:

$$\begin{aligned} \mathbf{G}^{f\#} \mathbf{A}^f &= \frac{1}{|Q^f|} \int_{Q^f} \mathbf{G} (\mathbf{I} - \nabla_y^t \chi) da \\ &= \frac{1}{|Q^f|} \int_{Q^f} (\text{div}_y \mathbf{G}^f) \otimes \tilde{\chi} da - \frac{1}{|Q^f|} \int_r \mathbf{G} v \otimes \tilde{\chi} dl \\ &= G^r \Psi \frac{\lambda_1}{\gamma_1} \mathbf{I} = \frac{2G^r \Psi}{1 + G^r g(1) W'_1(1)/G^m} \mathbf{I}. \end{aligned} \quad (117)$$

The tensor $\mathbf{G}^{f\#} = G^r \Psi \mathbf{I}$ is the average stiffness tensor of the fibre, taking into account the fibre grading features. It is pointed out that

(116) and (117) lump the fibre grading and anisotropy features into the coefficients $W'_1(1)$ and Ψ , which can be evaluated in closed form for the grading profiles considered in Section 4.

On the other hand, any numerical method to integrate (33)–(35) can yield $W'_1(1)$ and Ψ , and hence \mathbf{A}^f and $\mathbf{G}^{f\#}$, for a general grading profile. Here the methods proposed by Kanaun and Kudriavtseva (1989) and Herve and Zaoui (1993), based on a piece-wise constant approximation of the grading profile $g(\rho)$, is briefly recalled. The interval (0,1) is partitioned into M equal subintervals; the function $g(\rho)$ is taken constant in each subinterval, so that the restriction of the solution $W_1(\rho)$ of (33) can be represented as $A_i \rho^\sigma + B_i \rho^{-\sigma}$ in the i th subinterval, with constants A_i, B_i to be determined, for $i = 1, \dots, M$. The scalars A_{i+1}, B_{i+1} can be related to A_i, B_i by imposing that $W_1(\rho)$ and $g(\rho)W'_1(\rho)$ are continuous at the boundary between the i th and $(i+1)$ th subintervals, respectively, by congruence and equilibrium. Noting that $B_1 = 0$ by the regularity requirement (34), and recalling the normalization condition (35), all the constants A_i, B_i can be computed and hence $W'_1(1)$ is obtained. Then, Ψ follows from (60).

A different method to treat the related problem of fibres with graded interfaces (Shen and Li, 2003, 2005; Sevostianov and Kachanov, 2007) is based on the idea of increasing the inclusion in an incremental, “differential” manner, with homogenization at each step. More specifically, a certain “current” radius $0 < r < R$ is considered, and then an incremental layer dr of the graded material is added, assuming that the inclusion of radius r is homogeneous (homogenized at the previous step). To find the corresponding increment of modulus of the equivalent homogeneous inclusion, this enlargement is modeled by placing the inclusion of radius r into a matrix that has the property $\mathbf{G}^f(r)$. Reasoning as in Sevostianov and Kachanov (2007), i.e., using the Hashin–Shtrikman lower bound for the incremental homogenization, and limiting the analysis to isotropic graded fibres, the following differential equation for the modulus $G^{f\#}$ of the equivalent homogeneous inclusion is obtained:

$$\frac{dG^{f\#}}{dr} = -\frac{1}{r} \frac{(G^{f\#}(r) - G^r(r))(G^{f\#}(r) + G^r(r))}{G^r(r)}, \quad (118)$$

complemented with the initial condition $G^{f\#}(0) = G^r(0)$. Then, the average stiffness tensor of the whole fibre is $G^{f\#}(R)\mathbf{I}$, and the single-fibre concentration factor is $2G^m\mathbf{I}/(G^m + G^{f\#}(R))$, obtained from (116) for an homogeneous, or homogenized, isotropic fibre.

After the single-fibre concentration factor \mathbf{A}^f and the average stiffness tensor of the fibre $G^{f\#}$ have been evaluated, homogenization can be accomplished by several approximate methods. For example, the effective field method (Kanaun and Levin, 1994) leads to:

$$G^\# = G^m\mathbf{I} + f(G^{f\#} - G^m\mathbf{I})\mathbf{A}^f[(1-f)\mathbf{I} + f\mathbf{A}^f]^{-1}. \quad (119)$$

Of course, other models (e.g., differential, self-consistent) could be used as well. Table 3 presents a comparison between the results supplied by the above cited methods for evaluating \mathbf{A}^f , $G^{f\#}$, $G^\#$, and the method proposed herein, for some fibre volume fractions. An excellent agreement is obtained for \mathbf{A}^f , $G^{f\#}$, whereas a fair agreement is obtained for $G^\#$. It is emphasized that the present periodic-homogenization method takes into account the geometry of the microstructure, yielding different results for square ($\varphi = \pi/2$) or hexagonal ($\varphi = \pi/3$) fibre arrangements, whereas the simplified homogenization methods assume a statistically-isotropic fibre distribution. Moreover, a by-product of the present method is the ex-

act point-wise computation of the shear stress distribution (Section 5.4), which can be very useful in applications.

5.3. Parametric analysis

The influence of the microgeometry parameters κ and φ is addressed in Fig. 4(a) and (b). In particular, rectangular geometries ($\varphi = \pi/2$) with various unit-cell aspect ratios κ are considered in Fig. 4(a), whereas rhombic geometries ($\kappa = 1$) with various values of the unit-cell skewness φ are considered in Fig. 4(b). Fibres are isotropic, exponentially graded with $\omega = 4$, a contrast factor $\xi = 50$ is assumed, and the fibre-matrix interface is perfect. The dimensionless principal effective upper ($G_1^\#$) and lower ($G_2^\#$) moduli are plotted versus the fibre volume fraction f . All curves are monotonically increasing, because fibres are stiffer than the matrix. Each curve terminates at the volume fraction corresponding to the relevant packaging limit; near that limit, the upper modulus is highly sensitive to the volume fraction.

The influence of the interface strength δ and of the grading intensity ω is investigated in Fig. 5(a) and (b). Fibres are isotropic, exponentially graded, and a contrast factor $\xi = 50$ is assumed. A regular hexagonal unit cell is considered, so that the effective behaviour is isotropic, and the dimensionless homogenized shear modulus $G^\# / G^m$ is plotted versus the fibre volume fraction f .

Different values of δ are considered in Fig. 5(a); the value $\delta = +\infty$ corresponds to the perfect interface condition, i.e., contin-

Table 3
Single-fibre concentration factor \mathbf{A}^f , average stiffness tensor of the fibre $G^{f\#}$, and dimensionless effective modulus $G^\#$. Material parameters: $\xi = 50$, $\sigma = 1$, $\delta = +\infty$. Grading type: exponential; grading intensity $\omega = 4$. Cell geometry (relevant for the present analysis only): $\kappa = 1$, $\varphi = \pi/3$ or $\varphi = \pi/2$. Method: K-K, 1989 – Kanaun and Kudriavtseva (1989); S-K, 2007 – Sevostianov and Kachanov (2007); Present analysis – Eq. (59).

| Fibre volume fraction | \mathbf{A}^f | $G^{f\#}$ | $G^\#$ | | | |
|-------------------------------------|----------------|-----------|--------|--------|--------|---------|
| | | | 0.25 | 0.50 | 0.75 | 0.90 |
| K-K, 1989, $M = 10$ | 0.0797 | 31.1501 | 1.7805 | 3.2262 | 6.8192 | 13.5955 |
| K-K, 1989, $M = 40$ | 0.0669 | 30.9333 | 1.6529 | 2.8768 | 6.0029 | 12.2487 |
| K-K, 1989, $M = 100$ | 0.0643 | 30.9210 | 1.6283 | 2.8089 | 5.8414 | 11.9731 |
| K-K, 1989, $M = 400$ | 0.0631 | 30.9188 | 1.6161 | 2.7753 | 5.7609 | 11.8346 |
| K-K, 1989, $M = 1000$ | 0.0628 | 30.9187 | 1.6137 | 2.7686 | 5.7448 | 11.8068 |
| S-K, 2007 | 0.0627 | 30.9187 | 1.6121 | 2.7641 | 5.7341 | 11.7883 |
| Present analysis, $\varphi = \pi/3$ | 0.0627 | 30.9187 | 1.5835 | 2.6506 | 5.3491 | 12.3423 |
| Present analysis, $\varphi = \pi/2$ | 0.0627 | 30.9187 | 1.5842 | 2.6950 | 6.8533 | – |

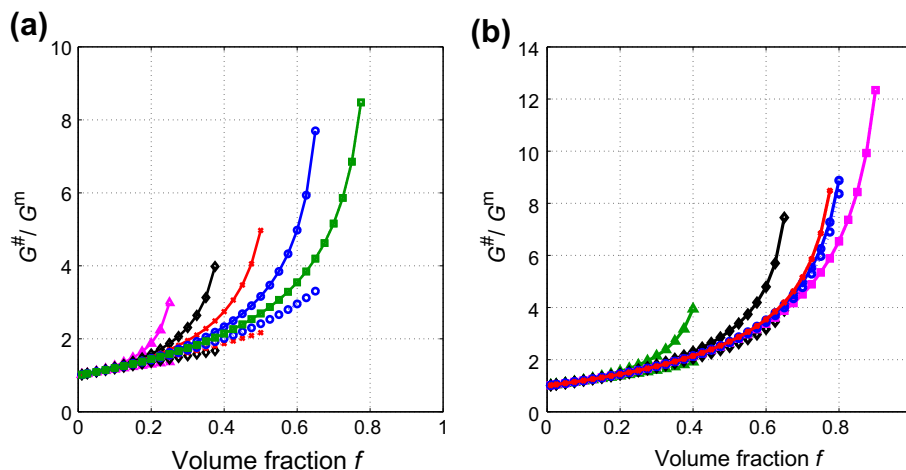


Fig. 4. Principal effective upper modulus $G_1^\#$ (continuous line) and lower modulus $G_2^\#$ (dotted line) versus fibre volume fraction f . Material parameters: $\xi = 50$, $\sigma = 1$, $\delta = +\infty$. Grading type: exponential; grading intensity $\omega = 4$. (a) Rectangular geometry: $\varphi = \pi/2$; $\kappa = 1$ – magenta squares, $\kappa = 1.2$ – blue circles, $\kappa = 1.5$ – red crosses, $\kappa = 2$ – black diamonds, $\kappa = 3$ – green triangles. (b) Rhombic geometry: $\kappa = 1$; $\varphi = \pi/6$ – green triangles, $\varphi = \pi/4$ – black diamonds, $\varphi = \pi/3$ – magenta squares, $\varphi = 5\pi/12$ – blue circles, $\varphi = \pi/2$ – red crosses. (For interpretation of the references to color in this figure legend, the reader is referred to the web version of this paper.)

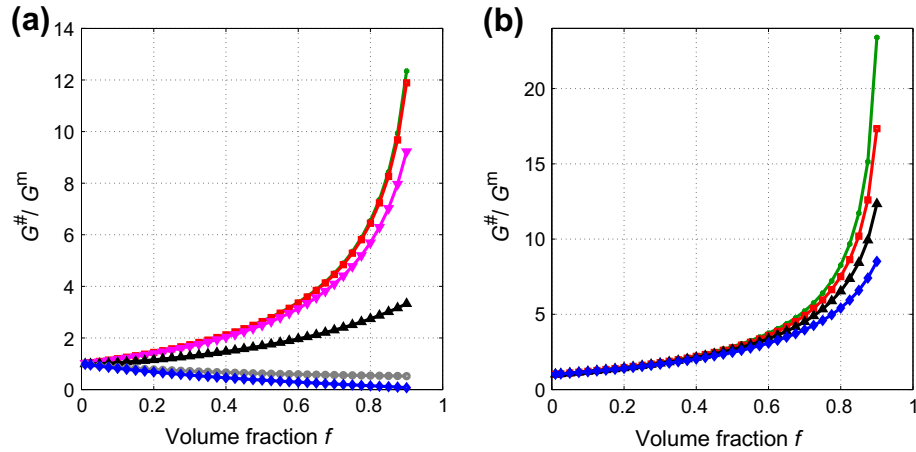


Fig. 5. Dimensionless effective modulus $G^\#$ versus fibre volume fraction f . Cell geometry: $\kappa = 1$, $\varphi = \pi/3$. Stiffness contrast factor: $\xi = 50$. Isotropic fibre: $\sigma = 1$. Grading type: exponential. (a) Influence of interface strength: $\delta = 0.1$ – blue diamonds, $\delta = 1$ – grey circles, $\delta = 10$ – black upper triangles, $\delta = 100$ – magenta lower triangles, $\delta = 1000$ – red squares, $\delta = +\infty$ – green stars. Grading intensity $\omega = 4$. (b) Influence of grading intensity: $\omega = 1$ – green stars, $\omega = 2$ – red squares, $\omega = 4$ – black triangles, $\omega = 8$ – blue diamonds. Perfect interface ($\delta = +\infty$). (For interpretation of the references to color in this figure legend, the reader is referred to the web version of this paper.)

uous displacement at interfaces. The homogenized shear modulus increases with the interface parameter, and over a certain limit ($\delta \cong 1000$) reaches saturation with no significant increase with respect to additional stiffening of the interface. On the opposite, a very weak interface, characterized by δ of the order of the unity or less, induces an effective modulus which results even lower than that of the matrix.

Different values of ω are considered in Fig. 5(b): the value $\omega = 1$ corresponds to homogeneous fibres; higher values of ω imply lower moduli at the fibre boundary, the stiffness at the fibre axis being constant. It turns out that the overall material modulus is scarcely influenced by ω at lower fibre volume fractions, whereas it significantly depends on the latter near the packaging limit.

Finally, Fig. 6 reports the influence of the fibre orthotropy parameter $\sigma^2 = G^0 / G^t$ on the dimensionless homogenized shear modulus $G^\# / G^m$. Fibres are exponentially graded with $\omega = 4$. A contrast factor $\xi = 50$ is assumed with perfect interface. Different values of σ^2 are considered. It is observed that progressively stiffer fibres along the θ direction imply a higher dimensionless modulus

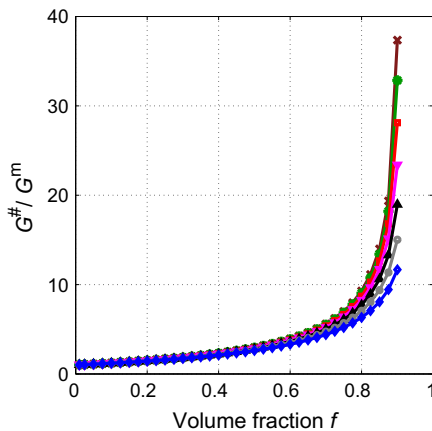


Fig. 6. Dimensionless effective modulus $G^\#$ versus fibre volume fraction f . Cell geometry: $\kappa = 1$, $\varphi = \pi/3$. Stiffness contrast factor: $\xi = 50$. Grading type: exponential. Grading intensity $\omega = 4$. Cylindrically orthotropic fibre. Influence of orthotropy parameter: $\sigma^2 = 1/8$ – blue diamonds, $\sigma^2 = 1/4$ – grey circles, $\sigma^2 = 1/2$ – black upper triangles, $\sigma^2 = 1$ – magenta lower triangles, $\sigma^2 = 2$ – red squares, $\sigma^2 = 4$ – green stars, $\sigma^2 = 8$ – brown x-marks. Perfect interface ($\delta = +\infty$). (For interpretation of the references to color in this figure legend, the reader is referred to the web version of this paper.)

$G^\# / G^m$ for each value of the fibre volume fraction f . The influence of σ^2 becomes significant near the packaging limit.

5.4. The shear stress concentration factor

In this section, the analysis points at assessing the reduction of shear stress concentration in the composite, by suitably choosing the grading intensity factor ω and the grading profile $g(\rho)$, keeping fixed the effective shear stiffness of the composite material.

Reference is made to a square cell geometry of volume fraction $f = 0.78$, i.e., with fibres nearly touching each others. The effective stiffness tensor $G^\#$ of the composite is isotropic. Perfect interfaces are assumed. Grading profiles with different features (e.g., concave, linear or convex) are considered in the computations and sketched in Fig. 7.

The point of view here is different from Fig. 5(b). The fibre/matrix stiffness ratio G^t / G^m was taken constant there, whereas the dimensionless effective shear stiffness $G^\# / G^m$ is taken constant here. Hence, the higher ω is, the higher G^t / G^m has to be chosen, in order to grant a fixed $G^\# / G^m$ value, since higher values of ω im-

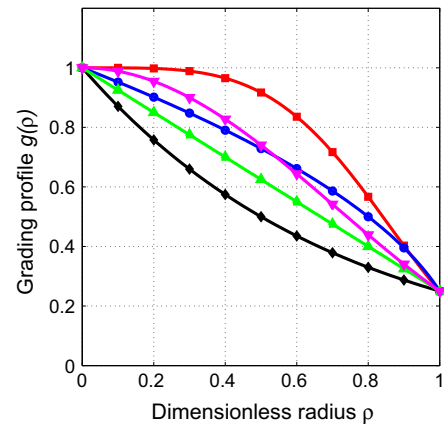


Fig. 7. Grading profiles $g(\rho)$ versus radial dimensionless coordinate ρ , for a grading intensity factor $\omega = 4$. Exponential profile (78) with $q = 1$ – black diamonds; exponential profile (78) with $q = 4$ – red squares; linear profile (108) with $v = 1$ – green triangles up; binomial-power-law profile (108) with $v = 1/2$ – blue circles; squared-first-kind-Bessel profile (93) with $v = 0$ – magenta triangles down. (For interpretation of the references to color in this figure legend, the reader is referred to the web version of this paper.)

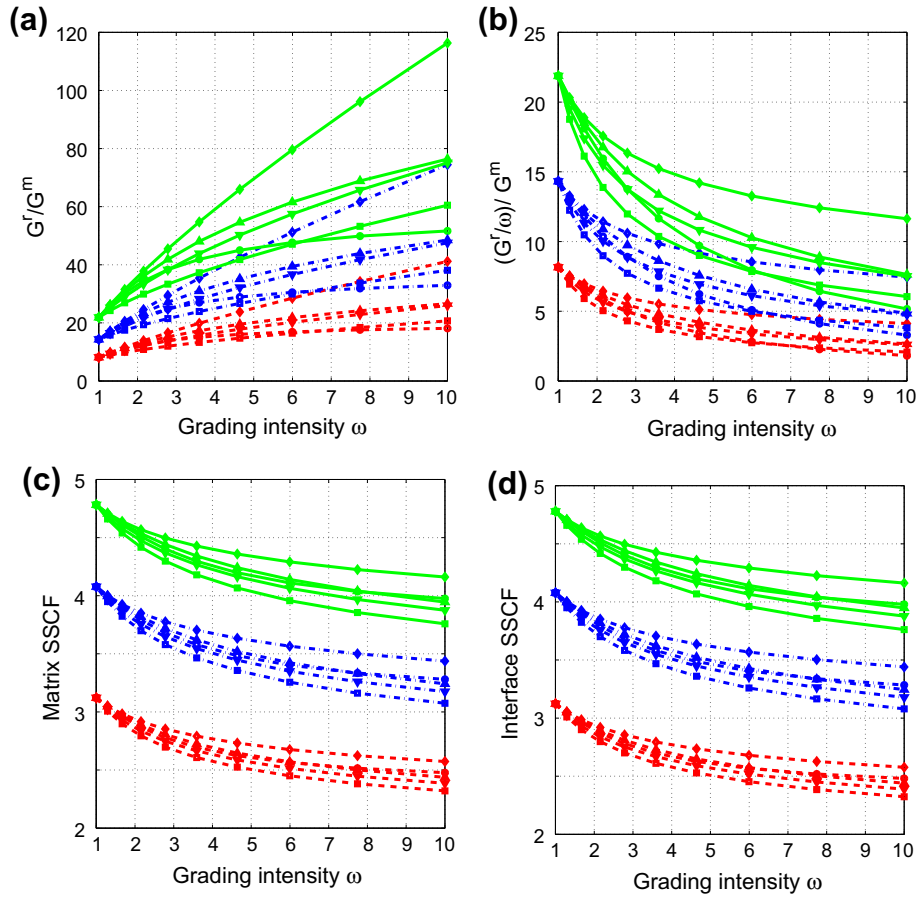


Fig. 8. (a) Axial (G^r/G^m) and (b) boundary ($(G^r/\omega)/G^m$) fibre/matrix stiffness ratio required to achieve a given dimensionless effective modulus $G^{\#}/G^m$, versus grading intensity ω . (c) Matrix and (d) Interface Shear Stress Concentration Factor (SSCF), versus grading intensity ω . $G^{\#}/G^m = 5$ – red dashed lines, $G^{\#}/G^m = 7.5$ – blue dash-dot lines, $G^{\#}/G^m = 10$ – green solid lines. Grading type: exponential profile with $q = 1$ – diamonds; exponential profile with $q = 4$ – squares; linear profile – triangles up; binomial-power-law profile with $\nu = 1/2$ – circles; squared-first-kind-Bessel profile with $\nu = 0$ – triangles down. Cell geometry: $\kappa = 1$, $\varphi = \pi/2$, $f = 0.78$. Material parameters: $\sigma = 1$, $\delta = +\infty$. (For interpretation of the references to color in this figure legend, the reader is referred to the web version of this paper.)

ply a steeper decrease of the fibre stiffness along the radius. This issue is shown in Fig. 8(a), reporting the values of G^r/G^m versus ω , that yield $G^{\#}/G^m = 5, 7.5$ or 10 , for each grading profile. In this way, classes of graded composites with the same effective stiffness are obtained.

Recalling that $g(0) = 1$ (Fig. 7), it follows that G^r/G^m is the fibre/matrix stiffness ratio computed at the fibre axis. The corresponding ratio computed at the fibre boundary, i.e., $(G^r/\omega)/G^m$, is reported in Fig. 8(b). Since these curves are decreasing, it follows that grading the fibre stiffness is a feasible way to reduce the stiffness contrast at the fibre-matrix interface, keeping constant the effective stiffness.

In fact, grading the fibre stiffness turns out to be a feasible way to mitigate the shear stress concentration in the composite. A quantitative account of this issue can be obtained by introducing the Shear Stress Concentration Factors (SSCFs). In particular, the matrix [respectively, fibre] SSCF is defined as the highest ratio between the L^∞ norm of the shear stress in the matrix [respectively, fibre] of the graded composite, and the same quantity in the homogenized material, under all the macroscopic shear strains $\nabla_x w_0$:

$$\text{Matrix SSCF} = \sup_{\nabla_x w_0} \frac{\sup_{(y_1, y_2) \in Q^m} |\tau_0(y_1, y_2)|}{G^{\#} |\nabla_x w_0|}, \quad (120)$$

where τ_0 is defined in (29) and $|\cdot|$ denotes the modulus. A similar equation holds for the fibre. Analogously, the interface SSCF is defined as the highest ratio between the L^∞ norm of the normal com-

ponent of the shear stress at the fibre-matrix interface in the graded composite, and the same quantity in the homogenized material, under all the macroscopic shear strains $\nabla_x w_0$:

$$\text{Interface SSCF} = \sup_{\nabla_x w_0} \frac{\sup_{\rho=1} |\tau_0 \cdot \nu|}{G^{\#} |\nabla_x w_0|}. \quad (121)$$

The matrix and interface SSCFs are reported in Fig. 8(c) and (d) as a function of ω , for $G^{\#}/G^m = 5, 7.5$ or 10 . The fibre SSCF coincides with the interface SSCF. A reduction of the shear stress of 25% for highly graded fibres ($\omega = 10$) with respect to homogeneous fibres ($\omega = 1$) is observed for all the levels of dimensionless homogenized modulus, when the exponential grading profile with $q = 4$ is chosen. Significant, though slightly lower, reductions are obtained also with other grading types. As a general trend, concave grading profiles tend to perform better than convex ones.

Hence, properly grading the elastic properties of the fibres leads to a decrease of the fibre, matrix and interfacial stress concentration, without reducing the overall stiffness of the material. This result raises attention on an innovative class of composite materials, enhanced in terms of durability of the matrix, the fibre and the bonding at the fibre-matrix interface.

6. Conclusion

This work dealt with the determination of the effective longitudinal shear moduli of a periodic composite material reinforced by

straight parallel circular fibres, made of cylindrically orthotropic material, graded along the fibre radius. The investigation was carried out by adopting the asymptotic homogenization theory. A closed-form expression of the effective shear moduli was obtained, for a wide class of grading profiles defined in terms of special functions and for a general unit cell geometry. The proposed method relies on the theory of Weierstrass elliptic functions for the satisfaction of local periodicity condition, and on the use of Fourier expansion for the solution of equilibrium equations. The present result was validated by means of comparison with finite element solutions on a set of representative benchmark cases and showed to be accurate, efficient and reliable. The numerical implementation of the proposed method exhibited exponential asymptotic convergence rate with respect to the truncation order of the involved series representations. The obtained analytical solution allowed for a parametric analysis focused on the geometrical, material and grading parameters that define a composite material. The analysis showed that suitably tuning such quantities is a feasible way to reduce the shear stress concentration in the composite. The reduction of the latter raised attention on the possibility of devising innovative composite materials, specifically designed to have better durability with respect to the risk of fibre or matrix failure, or fibre-matrix debonding. The present results apply also to other physical models, such as electric or thermal conduction problems, or electrostatics.

Acknowledgements

This work was developed within the framework of Lagrange Laboratory, a European research group comprising CNRS, CNR, the Universities of Rome “Tor Vergata”, Calabria, Cassino, Pavia, and Salerno, École Polytechnique, University of Montpellier II, ENPC, LCPC, and ENTPE.

References

- Abramowitz, M., Stegun, I.A., 1965. Handbook of Mathematical Functions with Formulas, Graphs and Tables. Dover, New York.
- Amar, M., Andreucci, D., Bisegna, P., Gianni, R., 2006. On a hierarchy of models for electrical conduction in biological tissues. *Math. Meth. Appl. Sci.* 29, 767–787.
- Apostol, T.M., 1997. Modular Functions and Dirichlet Series in Number Theory, second ed. Springer, New York.
- Bensoussan, A., Lions, J.-L., Papanicolaou, G., 1978. Asymptotic Analysis for Periodic Structures. North-Holland, Amsterdam.
- Benveniste, Y., Miloh, T., 2001. Imperfect soft and stiff interfaces in two-dimensional elasticity. *Mech. Mater.* 33, 309–323.
- Bigoni, D., Serkov, S.K., Valentini, M., Movchan, A.B., 1998. Asymptotic models of dilute composites with imperfectly bonded inclusions. *Int. J. Solids Struct.* 35 (24), 3239–3258.
- Bisegna, P., Caselli, F., 2008. A simple formula for the effective complex conductivity of periodic fibrous composites with interfacial impedance and applications to biological tissues. *J. Phys. D* 41, 115506 (13pp).
- Bonnet, G., 2007. Effective properties of elastic periodic composite media with fibers. *J. Mech. Phys. Solids* 55, 881–899.
- Chen, T., Kuo, H.-Y., 2005. Transport properties of composites consisting of periodic arrays of exponentially graded cylinders with cylindrically orthotropic materials. *J. Appl. Phys.* 98, 033716.
- COMSOL AB, 2008. Comsol Multiphysics® User's Guide (version 3.5). Available from: <<http://www.comsol.com>>.
- Genin, G.M., Birman, V., 2009. Micromechanics and structural response of functionally graded, particulate-matrix, fiber-reinforced composites. *Int. J. Solids Struct.* 46, 2136–2150.
- Gu, G., Liu, Z., 1992. Effects of contact resistance on thermal conductivity of composite media with a periodic structure. *J. Phys. D* 25, 249–255.
- Gu, G.Q., Yu, K.W., 2003. Conductivities of dilute suspensions of graded fibers. *J. Appl. Phys.* 94, 3376–3383.
- Hashin, Z., 1991. The spherical inclusion with imperfect interface. *J. Appl. Mech.* 58, 444–449.
- Hashin, Z., 2002. Thin interphase/imperfect interface in elasticity with application to coated fiber composites. *J. Mech. Phys. Solids* 50, 2509–2537.
- Helsing, J., 1995. An integral equation method for elastostatics of periodic composites. *J. Mech. Phys. Solids* 43, 815–828.
- Herve, E., Zaoui, A., 1993. *n*-Layered inclusion-based micromechanical modeling. *Int. J. Eng. Sci.* 31, 1–10.
- Iwakuma, T., Nemat-Nasser, S., 1983. Composites with periodic microstructure. *Comput. Struct.* 16, 13–19.
- Jiang, C.P., Xu, Y.L., Cheung, Y.K., Lo, S.H., 2004. A rigorous analytical method for doubly periodic cylindrical inclusions under longitudinal shear and its applications. *Mech. Mater.* 36, 225–237.
- Kalamkarov, A.L., 1992. Composite and Reinforced Elements of Construction. Wiley, Chichester.
- Kanaun, S.K., Kudriavtseva, L.T., 1989. Elastic and thermoelastic characteristics of composites reinforced with unidirectional fibre layers. *Appl. Math. Mech.* 53, 628–636.
- Kanaun, S.K., Levin, V.M., 1994. The self-consistent field method in mechanics of matrix composite materials. In: Markov, K.Z. (Ed.), *Advances in Mathematical Modelling of Composite Materials*. World Scientific Publisher, Singapore, pp. 1–58.
- Kantor, Y., Bergman, D.J., 1982. Elastostatic resonances – a new approach to the calculation of the effective elastic constants of composites. *J. Mech. Phys. Solids* 30, 355–376.
- Kushch, V.I., Sevostianov, I., Mishnaevsky Jr., L., 2008. Stress concentration and effective stiffness of aligned fiber reinforced composite with anisotropic constituents. *Int. J. Solids Struct.* 45, 5103–5117.
- Lene, F., Leguillon, D., 1982. Homogenized constitutive law for a partially cohesive composite material. *Int. J. Solids Struct.* 18, 443–458.
- Lutz, M.P., Zimmerman, R.W., 1996. Effect of the interphase zone on the bulk modulus of a particulate composite. *ASME J. Appl. Mech.* 8 (63), 855–861.
- Lutz, M.P., Zimmerman, R.W., 2005. Effect of an inhomogeneous interphase zone on the bulk modulus and conductivity of a particulate composite. *Int. J. Solids Struct.* 42, 429–437.
- Martin, P.A., 2002. On functionally graded balls and cones. *J. Eng. Math.* 42, 133–142.
- Meguid, S.A., Kalamkarov, A.L., 1994. Asymptotic homogenization of elastic composite with a regular structure. *Int. J. Solids Struct.* 31 (3), 303–316.
- Michel, J.C., Moulinec, H., Suquet, P., 1999. Effective properties of composite materials with periodic microstructure: a computational approach. *Comput. Meth. Appl. Mech. Eng.* 172, 109–143.
- Milton, G.W., 2004. The theory of composites. Cambridge Monographs on Applied and Computational Mathematics, vol. 6. Cambridge University Press, Cambridge.
- Mura, T., 1987. *Micromechanics of Defects in Solids*, second ed.. Mechanics of Elastic and Inelastic Solids Martinus Nijhoff Publishers, Dordrecht.
- Nicorovici, N.A., McPhedran, R.C., Milton, G.W., 1993. Transport properties of a three-phase composite material: the square array of coated cylinders. *Proc. Roy. Soc. Lond. A* 442, 599–620.
- Parnell, W.J., Abrahams, I.D., 2006. Dynamic homogenization in periodic fibre reinforced media. Quasi-static limit for SH waves. *Wave Motion* 43, 474–498.
- Perrins, W.T., McKenzie, D.R., McPhedran, R.C., 1979. Transport properties of regular arrays of cylinders. *Proc. Roy. Soc. Lond. A* 369, 207–225.
- Rayleigh, Lord, 1892. On the influence of obstacles arranged in rectangular order upon the properties of a medium. *Philos. Mag.* 34, 481–502.
- Reiter, T., Dvorak, G.J., Tvergaard, V., 1997. Micromechanical models for graded composite materials. *J. Mech. Phys. Solids* 45, 1281–1302.
- Rodríguez-Ramos, R., Sabina, F.J., Guinovart-Díaz, R., Bravo-Castillero, J., 2001. Closed-form expressions for the effective coefficients of a fiber-reinforced composite with transversely isotropic constituents – I. Elastic and square symmetry. *Mech. Mater.* 33, 223–235.
- Sanchez-Palencia, E., 1980. *Non-Homogeneous Media and Vibration Theory*. Lecture Notes in Physics. Springer, Berlin.
- Sevostianov, I., Kachanov, M., 2007. Effect of interphase layers on the overall elastic and conductive properties of matrix composites. Applications to nanosize inclusion. *Int. J. Solids Struct.* 44, 1304–1315.
- Shabana, Y.M., Noda, N., 2008. Numerical evaluation of the thermomechanical effective properties of a functionally graded material using the homogenization method. *Int. J. Solids Struct.* 45, 3494–3506.
- Shen, L., Li, J., 2003. Effective elastic moduli of composites reinforced by particle or fiber with an inhomogeneous interphase. *Int. J. Solids Struct.* 40, 1393–1409.
- Shen, L., Li, J., 2005. Homogenization of a fibre/sphere with an inhomogeneous interphase for the effective elastic moduli of composites. *Proc. Roy. Soc. Lond. A* 461, 1475–1504.
- Suresh, S., 1997. Modeling and design of multi-layered and graded materials. *Prog. Mater. Sci.* 42, 243–251.
- Suresh, S., 2001. Graded materials for resistance to contact deformation and damage. *Science* 292, 2447–2451.
- Tricomi, F.G., 1965. *Funzioni Speciali*. Editrice Tirrenia, Torino.
- Wei, E.-B., Song, J.-B., Tian, J.-W., 2003. Dielectric response of composites with graded cylindrical particles. *J. Phys.: Condens. Matter* 15, 8907–8915.
- Wei, E.-B., Gu, G.-Q., Yu, K.-W., 2006. Dielectric responses of graded composites having generalized gradation profiles. *Chin. Phys.* 15, 182–189.
- Whittaker, E.T., Watson, G.N., 1927. *A Course of Modern Analysis*. Cambridge University Press, Cambridge.